Copyright Warning & Restrictions

The copyright law of the United States (Title 17, United States Code) governs the making of photocopies or other reproductions of copyrighted material.

Under certain conditions specified in the law, libraries and archives are authorized to furnish a photocopy or other reproduction. One of these specified conditions is that the photocopy or reproduction is not to be "used for any purpose other than private study, scholarship, or research." If a, user makes a request for, or later uses, a photocopy or reproduction for purposes in excess of "fair use" that user may be liable for copyright infringement,

This institution reserves the right to refuse to accept a copying order if, in its judgment, fulfillment of the order would involve violation of copyright law.

Please Note: The author retains the copyright while the New Jersey Institute of Technology reserves the right to distribute this thesis or dissertation

Printing note: If you do not wish to print this page, then select "Pages from: first page # to: last page #" on the print dialog screen

ABSTRACT

THE MECHANICAL TESTING OF SINGLE NANOFIBER

by

Pratik Manohar Dahule

Polymer nanofibers exhibit properties that make them a favorable material for the development of tissue engineering scaffolds, filtration devices, sensors, and high strength lightweight materials. Perfectly aligned PLLA Nanofibers were fabricated by an electrospinning technique under optimum conditions and the diameter of the electrospun fibers can easily be tailored by adjusting the concentration of the polymer solution. To align the nanofibers, special arrangement was made in terms of two aluminum plates. Good alignment of polymer nanofibers on specimen was confirmed by SEM observation. The effect of different electro-spinning parameters on maximum fiber length, average fiber diameter, diameter uniformity, and fiber quality was explored in this study. The force applied on the nanofiber was measured with the help of AFM by satisfying Hooke's Law. The elastic properties of PLLA nanofiber were investigated with the atomic force microscope (AFM). The elasticity was calculated by analyzing the recorded force curves with the help of the Hertz model. Mechanical testing confirmed that the single aligned nanofiber can be an advancement in the commercial applications of nanofibers.

THE MECHANICAL TESTING OF SINGLE NANOFIBER

by

Pratik Manohar Dahule

Thesis
Submitted to the Faculty of
New Jersey Institute of Technology
In Partial Fulfillment of the Requirements for the Degree of
Master of Science in Mechanical Engineering

Department of Mechanical Engineering

January 2012

APPROVAL PAGE

THE MECHANICAL TESTING OF SINGLE NANOFIBER

Pratik Manohar Dahule

Dr. Michael Jaffe, Thesis Advisor Research Professor of Biomedical Engineering, NJIT	Date
Dr. Kwabena A Narh, Co Advisor Professor of Mechanical Engineering, NJIT	Date
Dr. Bryan Pfister, Committee Member Associate Professor of Biomedical Engineering, NJIT	Date
Dr. George Collins, Committee Member Research Professor of Biomedical Engineering, NJIT	Date

BIOGRAPHICAL SKETCH

Author: Pratik Manohar Dahule

Degree: Master of Science

Date: January 2012

Undergraduate and Graduate Education:

- Master of Science in Mechanical Engineering,
  New Jersey Institute of Technology, Newark, NJ, 2012

- Bachelor of Science in Mechanical Engineering,
  Amravati University, Pusad, India, 2009

Major: Mechanical Engineering

"Aum Shri GuruDev Dutt"

This thesis is dedicated to my father and mother who always stood behind me and gave me so much of support every time. I am thankful to all my family, teachers and friends who made me capable of reaching this point.

ACKNOWLEDGMENT

I would like to thank Dr. Michael Jaffe for not only being my advisor but also a guardian who gave me good advices during my thesis and curriculum. I also express my gratitude to Dr. George Collins who guided me with my research work. I would like to thank Dr. Kwabena Narh and Dr. Bryan Pfister for being my committee members and showing interest in my thesis. I am grateful to Ms. Xueyan Zhang for guiding and training me in characterization technique, without which this research work would not have been possible.

Last, but not the least, I would like to thank my family and my friends, Tanmay Pathre, Harshil Poojara, Sampath, Arun, Anil Shrirao, Abhishek Bhagwat, Samarth Trivedi, Tamil, Pranav Dahule, Mukul Bapat, Sandeep Singh, Pritam and others who diligently helped me throughout my research work.

TABLE OF CONTENTS

TABLE OF CONTENTS
(Continued)

LIST OF TABLES

Table **Page**

LIST OF FIGURES

LIST OF FIGURES
(Continued)

Figures **Page**

CHAPTER 1

INTRODUCTION

Nanotechnology is the study of manipulating matter on an atomic and molecular scale. Generally, nanotechnology deals with developing materials, devices, or other structures possessing at least one dimension sized from 1 to 100 nanometers. Nanotechnology is the science and engineering of creating materials, functional structures and devices on a nanometer scale, corresponding to a length of 10^{-9} m. The fascination of downsizing materials to nanoscale dimensions comes from scientific observations of considerable change in fundamental mechanical, physical, chemical and biological properties as a function of their size, shape, surface chemistry and topology. Therefore, nanotechnology has generated growing interest in the scientific community, and it has become a very active area of research.

A polymeric fiber is a polymer whose aspect ratio is greater than 100. The production of fibers from organic polymers involves forming the polymer into filaments and extending them uniaxially in order to orient molecules in the direction of the applied strain [1]. Conventional methods of polymer fiber production include melt spinning, solution spinning and gel state spinning. These methods rely on mechanical forces to produce fibers by extruding polymer melt or solution through a spinneret and subsequently drawing the resulting filaments as they solidify or coagulate. By using these methods, typical fiber diameters in the range of 5 to 500 microns can be produced. The consistently producible minimum fiber diameter is on the order of a micron [2].

Though there are many methods of fiber production, Electrospinning is a much reported, but to date minimally commercialized process to generate smaller fibers. Electrospinning was first patented in 1897 and used in the textile industry in the 1930s [3]. Electrospinning is a unique method that produces polymer fibers with diameter in the range of nanometer to a few microns using electrically driven jet of polymer solution or melt [4, 5]. This technique has been developed since introduced by Formhals in 1934 [3]. It did not gain significant industrial importance in the past due to the low output of the process, inconsistent and low molecular orientation, poor mechanical properties and high diameter distribution of the electrospun fibers. The electrospinning process itself begins with a solution of polymers, long chains of molecules, pumped into an electrified metal nozzle. High voltage creates a cone of fluid outside the nozzle, and a tiny jet of material erupts, electrically attracted to a target surface a few inches below the nozzle. In a few milliseconds, the electric field aligns the polymer molecules in the jet stream into fibrous strands, pulling and stretching the jet 1,000 times thinner than the micron-sized nozzle opening, to about diameters in the nanometer range [3].

Electrospun fibers have nanostructured surface morphologies with tiny pores that influence mechanical property like Young's modulus. As it is evident, there is less information available on the mechanical properties of nanofibers. Research on the mechanical properties of nanofibers from a variety of polymers is essential for a greater understanding on the contributions of nanofibers to the mechanical and performance related characteristics of nanofiber. Nanofibers have been attracting the attention of global materials research these days primarily due to their enhanced properties required for application in specific areas like catalysis, filtration, nano electro-mechanical system

(NEMS), nanocomposites, nanofibrous structures, tissue scaffolds, drug delivery systems, protective textiles, storage cells for hydrogen fuel cells, etc. Carbon nanofibers are finding enormous applications in unconventional energy sources and storage cells, due to their enhanced conductivity and high aspect ratio. Their mechanical properties enable them to be used as fillers in composites that find applications in synthetic and rubber industries. Carbon nanofiber reinforced composites offer increased stiffness, high strength and low electrical resistivity. Also, aligned nanofiber composites provide enhanced mechanical properties than the randomly aligned nanofiber composite structure.

The electrospun nanofibers provide a very large surface area/mass due to their small diameter, hence non-woven fabrics, with small fibers can be used for filtration of sub-particles in the separation industry. These can also be used for the adsorption of biological and chemical warfare gases, protective clothing, in medical industry as artificial blood vessels, sutures, surgical facemask, fiber-reinforced materials, monodirectional composites and in agricultural field for control of pesticides. The electrospinning technique can be used in chemical and manufacturing industries for paint spraying, electro deposition, plasma deposition, and mining minerals. In general, polymer nanofibers are used in a variety of applications, including filtration, protective clothing, biomedical applications such as wound dressing and drug delivery systems, design of solar cells, light cells and mirrors for use in space, as well as for structural elements in artificial organs and in reinforced composites. Ceramic or carbon nanofibers made from polymer precursors make it possible to expand the list of possible uses for nanofibers. Another promising field of application of nanofibers is tissue engineering. Synthetic tissues help stimulate living tissues to repair themselves in various parts of the human

body, such as cartilage, blood vessels, bones and so forth, due to diseases or wear and tear. Victims whose skin are burned or scalded by fire or boiling water may also find an answer in synthetic tissues. The newest generation of synthetic implant materials, also called biomaterials, may even treat diseases such as Parkinson's, arthritis and osteoporosis.

In this study, nanofiber was produced by electrospinning poly L (lactides), their morphology was characterized with the help of Scanning Electron Microscope and mechanical characterization was done with the help of Atomic Force Microscope.

CHAPTER 2

BACKGROUND

A number of processing techniques such as drawing, template synthesis, phase separation, self-assembly, electrospinning have been used to prepare polymer nanofibers in recent years. According to Zheng-Ming Huang [6] the electrospinning process is the only method, which can be further developed for mass production of one-by-one continuous nanofibers from various polymers. Despite possessing these unique features, one of the main challenges in this area is to characterize the mechanical behavior of the nanofibers. This could be due to the difficulty in handling the nanofibers and also due to the low load required for the deformation. Hence, in most cases, the mechanical integrity of the fibers is least understood and an understanding of the phenomenon is urgently needed. In most of the applications, the nanofibers are subjected to stresses and strains from surrounding media during their service lifetime. Such stresses can cause permanent deformation and even failure to the nanofibers. Therefore there is a need to characterize the mechanical properties of nanofiber [7].

2.1 Electrospinning History

The electrostatic spray literature contains many helpful insights into the electrospinning process. Lord Raleigh [8] studied the instabilities that occur in electrically charged liquid droplets. He showed, over 100 years ago, that when the electrostatic force overcame the surface tension, a liquid jet was created. Zeleny [9] considered the role of surface instabilities in electrical discharges from drops. He published a series of papers around

1910 on discharges from charged drops falling in electric fields, and showed that, when the discharge began, the theoretical relations for the surface instability were satisfied. In 1952, Vonnegut and Neubaur [10] produced uniform streams of highly charged droplets with diameters of around 0.1mm, by applying potentials of 5 to 10 kilovolts to liquids flowing from capillary tubes. Their experiment proved that monodisperse aerosols with a particle radius of a micron or less could be formed from pendent droplet at the end of the pipette. The diameter of the droplet was sensitive to the applied potential. Wachtel and coworkers [11] prepared emulsion particles using 45 electrostatic methods to make a monodisperse emulsion of oil in water. The diameters of the emulsion particles were from 0.5 to 1.6 microns. In 1960's Taylor [12] studied the disintegration of water droplets in an electric field. His theoretical papers demonstrated that a conical interface, with a semi-angle close to 49.3°, was the limiting stable shape.

Gladding [13] and Simons [14] improved the electrospinning apparatus and produced more stable fibers. They used movable devices such as a continuous belt for collecting the fibers. Later, Bornat [15] patented another electro-spinning apparatus that produced a removable sheath on a rotating mandrel. The basic principles were similar to previous patents. He determined that the tubular product obtained by electrospinning polyurethane materials in this way could be used for synthetic blood vessels and urinary ducts.

In 1971, electrospinning of acrylic fibers was described by Baumgarten [16]. Acrylic polymers were electrospun from dimethylformamide solution into fibers with diameters less than 1 micron. A stainless steel capillary tube was used to suspend the drop of polymer solution and the electrospun fibers were collected on a grounded metal

screen. Baumgarten observed relationships between fiber diameter, jet length, solution viscosity, feed rate of the solution and the composition of the surrounding gas.

In 1981, Manley and Larrondo [17] reported that continuous fibers of polyethylene and polypropylene could be electrospun from the melt, without mechanical forces. A drop of molten polymer was formed at the end of a capillary. A molten polymer jet was formed when high electric field was established at the surface of the polymer. The jet became thinner and then solidified into a continuous fiber. The molecules in the fiber were oriented by an amount similar to that found in conventional as-spun textile fibers before being drawn. The fiber diameter depended on the electric field, the operating temperature and the viscosity of the sample. X-ray diffraction and mechanical testing characterized the electrospun fibers. As either the applied electric field or the take-up velocity was increased, the diffraction rings became arcs, showing that the molecules were elongated along the fiber axis.

Reneker and coworkers [18] made further contributions to understanding the electro-spinning process and characterizing the electrospun nanofibers in recent years. Doshi [19] made electrospun nanofibers, from water-soluble poly (ethylene oxide), with diameters of .05 to 5 microns. He described the electrospinning process, the processing conditions, fiber morphology and some possible uses of electrospun fibers. Srinivasan [20] electro-spun a liquid crystal polyaramid, poly (p-phenylene terephthalamide), and an electrically conducting polymer, poly(aniline), each from solution in sulfuric acid. He observed electron diffraction patterns of polyaramid nanofibers both as spun and after annealing at 400°C. Chun [21] used transmission electron microscopy, scanning electron microscopy and atomic force microscopy to characterize electrospun fibers of poly

(ethylene terephthalate). Fang [22] electrospun DNA into nanofibers, some of which were beaded.

2.2 The Electrospinning Process

Electrospinning is a unique approach using electrostatic forces to produce fine fibers. Electrostatic precipitators and pesticide sprayers are some of the well known applications that work similarly to the electrospinning technique. Fiber production using electrostatic forces has invoked glare and attention due to its potential to form fine fibers. Electrospun fibers have small pore size and high surface area. There is also evidence of sizable static charges in electrospun fibers that could be effectively handled to produce three dimensional structures [23].

According to the authors of article [21], electrospinning is a process by which a polymer solution or melt can be spun into smaller diameter fibers using a high potential electric field. This generic description is appropriate as it covers a wide range of fibers with submicron diameters that are normally produced by electrospinning. Based on earlier research results, it is evident that the average diameter of electrospun fibers ranges from 100 nm–500 nm. In textile and fiber science related scientific literature, fibers with diameters in the range 100 nm–500 nm are generally referred to as nanofibers. The advantages of the electrospinning process are its technical simplicity and its easy adaptability. The apparatus used for electrospinning is simple in construction, which consists of a high voltage electric source with positive or negative polarity, a syringe pump with capillaries or tubes to carry the solution from the syringe or pipette to the

spinnerette, and a conducting collector like aluminum. The collector can be made of any shape according to the requirements, like a flat plate, rotating drum, etc.

Polymer solution or the melt that has to be spun is forced through a syringe pump to form a pendant drop of the polymer at the tip of the capillary. High voltage potential is applied to the polymer solution inside the syringe through an immersed electrode, thereby inducing free charges into the polymer solution. These charged ions move in response to the applied electric field towards the electrode of opposite polarity, thereby transferring tensile forces to the polymer liquid [21]. At the tip of the capillary, the pendant hemispherical polymer drop takes a cone like projection in the presence of an electric field. And, when the applied potential reaches a critical value required to overcome the surface tension of the liquid, a jet of liquid is ejected from the cone tip [12].

Most charge carriers in organic solvents and polymers have lower mobilities, and hence the charge is expected to move through the liquid for larger distances only if given enough time. After the initiation from the cone, the jet undergoes a chaotic motion or bending instability and is field directed towards the oppositively charged collector, which collects the charged fibers [24]. As the jet travels through the atmosphere, the solvent evaporates, leaving behind a dry fiber on the collecting device. For low viscosity solutions, the jet breaks up into droplets, while for high viscosity solutions it travels to the collector as fiber jets [25].

2.2.1 Electrospinning Technology: Current Scenario

There has been a substantial amount of research carried out on the fundamental aspects of electrospinning. The major issue that is yet to be resolved is the scaling-up of the process for commercialization. Academic and research communities should join hands in taking the lab-scale technology to the commercial level. A succinct summary on nanofiber research that is of use to the fiber and textile industry has been provided by Shastri and Ramkumar [26].

Electrospinning apparatus is simple in construction, and there have been no significant developments in the equipment design in the last decade. Research groups have improvised the basic electrospinning setup to suit their experimental needs and conditions. Warner et al. [27] have designed a new parallel plate setup for effectively controlling the operating variables to quantify the electro hydrodynamics of the process. The parallel plate design is expected to overcome the problem of a nonuniform electric field experienced in the point plate configuration. Jaeger et al. have used a two electrode setup by placing an additional ring electrode in front of the capillary to reduce the effect of the electrostatic field at the tip and to avoid corona discharges [28]. It has been stipulated that by using the two electrode setup, a more stable field can be established between the ring electrode and the collector, thereby avoiding the effect of changing shape at the capillary tip over the electric field.

Productivity enhancement for commercializing the electrospinning process is under active research, with emphasis on multiple spinneret designs and alternative experimental setup for feed charging. However, there is still a debate on the potential of

scaling up this technology for commercialization. There are only a few technology companies engaged in research and development on nanofibers. There is hardly any information available in the public domain on the mass production of nanofibers for different applications. Espin Technologies, a nanofiber technology company, is involved in developing a proprietary high speed device that could effectively overcome the traditional drawbacks of low output and high production cost [29].

Donaldson filtration Company has its own patented process setup for making tens of thousands of square meters of electrospun nanofiber filter media [30]. From the available published literature and the current state of understanding of the electrospinning process, it is likely that commercial scaling up of the electrospinning process can only be achieved by more fundamental understanding of the process and better control of the instability behavior of the jets that determine the diameter of the fibers. In addition, there needs to be an active participation between government agencies, industry, and academia for scaling-up the process. With greater enthusiasm among the interested parties, programs that are in place, such as Grants Opportunities for Academic Liaison with Industry of the NSF and SBIR programs, can be of assistance for technology transfer and commercialization.

2.2.2 Spinning of Polymeric Nanofibers

Research activity on the electrospinning of nanofibers has been successful in spinning submicron range fibers from different polymeric solutions and melts. Although a plethora of literature is available on the structure and morphological properties of polymeric nanofibers, there is very little information in the public domain on the electro

hydrodynamics of the electrospinning process. Polymers with attractive chemical, mechanical, and electrical properties like high conductivity, high chemical resistance, and high tensile strength have been spun into ultrafine fibers by the electrospinning process, and their application potential in areas like filtration, optical fibers, drug delivery system, tissue scaffolds, and protective textiles have been examined [25, 31].

2.2.3 Structure and Morphology of Polymeric Nano-fibers

In recent times, nanofibers have attracted the attention of researchers due to their pronounced micro and nano structural characteristics that enable the development of advanced materials that have sophisticated applications. More importantly, high surface area, small pore size, and the possibility of producing three dimensional structures have increased the interest in nanofibers. As theoretical studies on the electrospinning process have been conducted by various groups [24, 32-38] for a while to understand the electrospinning process, there have been some simultaneous efforts to characterize the structure and morphology of nanofibers as a function of process parameters and material characteristics.

The production of nanofibers by the electro-spinning process is influenced both by the electrostatic forces and the viscoelastic behavior of the polymer. Process parameters, like solution feed rate, applied voltage, nozzle-collector distance, and spinning environment, and material properties, like solution concentration, viscosity, surface tension, conductivity, and solvent vapor pressure, influence the structure and properties of electrospun nanofibers. Significant work has been done to characterize the properties of fibers as a function of process and material parameters. A detailed account on the

influence of process and material characteristics on the structure and properties of nanofibers is provided in the following sections of this paper.

2.2.4 Process Parameters and Fiber Morphology

Applied voltage

Various instability modes that occur during the fiber forming process are expected to occur by the combined effect of both the electrostatic field and the material properties of the polymer. It has been suggested that the onset of different modes of instabilities in the electrospinning process depend on the shape of the jet initiating surface and the degree of instability, which effectively produces changes in the fiber morphology [25]. In electrospinning, the charge transport due to the applied voltage is mainly due to the flow of the polymer jet towards the collector, and the increase or decrease in the current is attributed to the mass flow of the polymer from the nozzle tip. Deitzel et al. have inferred that the change in the spinning current is related to the change in the instability mode [25]. They experimentally showed that an increase in applied voltage causes a change in the shape of the jet initiating point, and hence the structure and morphology of fibers. Experimentation on a PEO/water system has shown an increase in the spinning current with an increase in the voltage [25].

It was also observed that for the PEO/water system, the fiber morphology changed from a defect free fiber at an initiating voltage of 5.5 kV to a highly beaded structure at a voltage of 9.0 kV [25]. The occurrence of beaded morphology has been correlated to a steep increase in the spinning current, which controls the bead formation in the

electrospinning process. Beaded structure reduces the surface area, which ultimately influence the filtration abilities of nanofibers.

Earlier in 1971, Baumgarten while carrying out experiments with acrylic fibers observed an increase in fiber length of approximately twice with small changes in fiber diameter with an increase in applied voltage [16]. Megelski et al. [39] investigated the voltage dependence on the fiber diameter using polystyrene (PS). The PS fiber size decreased from about 20 m to 10 m with an increase in voltage from 5 kV to 12 kV, while there was no significant change observed in the pore size distribution. These results concur with the interpretation of Buchko et al., [40] who observed a decrease in the fiber diameter with an increase in the applied field while spinning silk like polymer fiber with fibronectin functionality (SLPF). Generally, it has been accepted that an increase in the applied voltage increases the deposition rate due to higher mass flow from the needle tip.

Jaeger et al. used a two-electrode setup for electrospinning by introducing a ring electrode in between the nozzle and the collector [28]. The ring electrode was set at the same potential as the electrode immersed in the polymer solution. This setup was thought to produce a field-free space at the nozzle tip to avoid changes in the shape of the jet initiating surface due to varied potential [28]. Though this setup reduces the unstable jet behavior at the initiation stage, bending instability is still dominant at later stages of the process, causing an uneven chaotic motion of the jet before depositing itself as a nonwoven matrix on the collector. Deitzel et al. experimented with a new electrospinning apparatus by introducing eight copper rings in series in between the nozzle and the collector for dampening the bending instability [41].

The nozzle and the ring set were subjected to different potentials (ring set at a lower potential) of positive polarity, while the collector was subjected to a negative polarity. The idea behind this setup was to change the shape of the macroscopic electric field from the jet initiation to the collection target in such a way that the field lines converge to a center line above the collection target by the applied potential to the ring electrodes. The authors have suggested that the bending instability of fibers was dampened by the effect of the converging field lines producing straight jets [41]. Controlled deposition helps to produce specific deposition patterns and also yarn like fibers. Deitzel et al. investigated the spinning of PEO in aqueous solution using multiple electric fields, which resulted in fibers depositing over a reduced area due to the dampening of bending instability. The multiple field technique was also shown to produce fibers of lesser diameter than the conventional electrospinning method [41].

Nozzle collector distance

The structure and morphology of electrospun fibers is easily affected by the nozzle to collector distance because of their dependence on the deposition time, evaporation rate, and whipping or instability interval. Buchko et al. examined the morphological changes in SLPF and nylon electrospun fibers with variations in the distance between the nozzle and the collector screen. They showed that regardless of the concentration of the solution, lesser nozzle-collector distance produces wet fibers and beaded structures. SLPF fiber morphology changed from round to flat shape with a decrease in the nozzle collector distance from 2cm to 0.5cm [40]. This result shows the effect of the nozzle collector distance on fiber morphology. The work also showed that aqueous polymer solutions require more distance for dry fiber formation than systems that use highly volatile organic

solvents [40]. Megelski et al. observed bead formation in electrospun PS fibers on reducing the nozzle to collector distance, while preserving the ribbon shaped morphology with a decrease in the nozzle to collector distance [39].

Polymer flow rate

The flow rate of the polymer from the syringe is an important process parameter as it influences the jet velocity and the material transfer rate. In the case of PS fibers, Megelski et al. observed that the fiber diameter and the pore diameter increased with an increase in the polymer flow rate [39]. As the flow rate increased, fibers had pronounced beaded morphologies and the mean pore size increased from 90 to 150 nm [39].

Spinning environment

Environmental conditions around the spinneret, like the surrounding air, its relative humidity (RH), vacuum conditions, surrounding gas, etc., influence the fiber structure and morphology of electrospun fibers. Baumgarden observed that acrylic fibers spun in an atmosphere of relative humidity more than 60% do not dry properly and get entangled on the surface of the collector [16]. The breakdown voltage of the atmospheric gases is said to influence the charge retaining capacity of the fibers [16]. Megelski et al. investigated the pore characteristics of PS fibers at varied RH and emphasized the importance of phase separation mechanisms in explaining the pore formation of electrospun fibers [39].

2.3 Common Biodegradable Polymers Used In Electrospinning

Biodegradable polymers can be either natural or synthetic. In general, synthetic polymers offer greater advantages than natural materials because they can be tailored to give a wider range of properties and more predictable uniformity than can materials from natural sources. Synthetic polymers also represent a more reliable source of raw materials, one free from concerns of immunogenicity.

2.3.1 Poly (lactides)

Poly (Lactic Acid) → **(--CO---CH (CH_3)—O--)$_n$**

Poly (Glycolic Acid) → **(--CO—CH_2—O--)$_n$**

Poly (Lactic Acid-co- Glycolic Acid) →

(--CO---CH (CH_3)—O--)$_x$-- (--CO—CH_2)$_y$--COOH

Poly (glycolic) acid (PGA) and poly (lactic acid) (PLA) are aliphatic polyesters of poly(α hydroxy acids). These polymers and their associated copolymers are perhaps the most common biodegradable synthetic polymers known and have been used in drug delivery, bone osteosynthesis and tissue engineering of skin [42]. PGA's relatively short chain length and polar properties give rise to its high crystallinity, melting point and low solubility in organic solvents [42]. PGA is also insoluble in the organic chloroform and dioxane solvents used in creating the scaffolds. This project is therefore unable to explore PGA polymer nonwoven webs.

As seen in the structures above, PLA has an extra chiral methyl group, making a D- or L- isomer possible. This extra methyl group also makes PLA more hydrophobic

than PGA. PLA is hydrophobic and films of PLA take up only about 2% water [42]. Due to steric hindrance of the methyl group, the ester bond of PLA is less likely to undergo hydrolysis, making the degradation time for PLA longer than its relative PGA and its copolymer PLGA. Other factors such as molecular weight, exposed surface area and crystallinity affect degradation rates as well [43]. PLLA and PDLLA degrade by simple hydrolysis of the ester bond linkage to yield L-lactic acid or D-lactic acid, respectively.

Table 2.1 Common Properties of Poly (Lactic Acid)

Polymers	**% Crystallinity**	**Expected T_m (°C)**	**Expected T_g (°C)**
PLLA	37	185	57
PDLLA	0	None	49

Because the L-lactic acid is a natural occurring stereoisomer of lactic acid, PLLA is used more often than PDLLA. However, crystallinity of the polymers also relates to their use. PDLLA is amorphous and therefore used in drug delivery applications that require uniform dispersion of species, while 37% crystalline PLA can often be found in orthopedic devices that require high mechanical strength and toughness [42].

PGA and PLA copolymers all release acidic products upon hydrolytic degradation. In studies done on in vivo response of these polymers, about 8% of patients have shown late inflammatory reaction [43]. Acidic degradation products may contribute to the inflammatory response and other polymers have been researched as a solution. One of these polymers is poly(ε-caprolactone), known as PCL [42].

2.4 Clinical and Industrial Applications of Nanofibers

From a biological viewpoint, almost all of the human tissues and organs are deposited in nano fibrous forms or structures. Examples include: bone, dentin, collagen, cartilage, and skin. All of them are characterized by well-organized hierarchical fibrous structures14 realigning in nanometer scale. According to the research conducted in the field of nanotechnology, compatibility has to do with the size of the fibers that make up the materials. As such, current research in electrospun polymer nanofibers has focused one of their major applications on bioengineering.

2.4.1 Medical Prostheses

Polymer nanofibers fabricated via electrospinning have been proposed for a number of soft tissue prostheses applications such as blood vessel, vascular, breast, etc. In addition, electrospun biocompatible polymer nanofibers can also be deposited as a thin porous film onto a hard tissue prosthetic device designed to be implanted into the human body. This coating film with gradient fibrous structure works as an interphase between the prosthetic device and the host tissues, and is expected to efficiently reduce the stiffness mismatch at tissue/device interphase and hence prevent the device failure after the implantation [44].

2.4.2 Tissue Engineering

For the treatment of tissues or organs in malfunction in a human body, one of the challenges to the field of tissue engineering is the design of ideal scaffolds/synthetic matrices that can mimic the structure and biological functions of the natural extracellular matrix (ECM). Human cells can attach and organize well around fibers with diameters smaller than those of the cells. In this regard, nanoscale fibrous scaffolds can provide an

optimal template for cells to seed, migrate, and grow. A successful regeneration of biological tissues and organs calls for the development of fibrous structures with fiber architectures beneficial for cell deposition and cell proliferation. Of particular interest in tissue engineering is the creation of reproducible and biocompatible three-dimensional scaffolds for cell ingrowths resulting in bio-matrix composites for various tissue repair and replacement procedures. Recently, people have started to pay attention to making such scaffolds with synthetic biodegradable polymer nanofibers. It is believed that converting biopolymers into fibers and networks that mimic native structures will ultimately enhance the utility of these materials, as large diameter fibers do not mimic the morphological characteristics of the native fibrils [44].

2.4.3 Wound Dressing

Polymer nanofibers can also be used for the treatment of wounds or bums of a human skin, as well as designed for haemostatic devices with some unique characteristics. With the aid of electric field, fine fibers of biodegradable polymers can be directly sprayed/spun onto the injured location of skin to form a fibrous mat dressing which can let wounds heal by encouraging the formation of normal skin growth and eliminate the formation of scar tissue, which would occur in a traditional treatment. Non-woven nanofibrous membrane mats for wound dressing usually have pore sizes ranging from 500 nm to 1 mm, small enough to protect the wound from bacterial penetration via aerosol particle capturing mechanisms. High surface area of 5-100 m^2/g is extremely efficient for fluid absorption and dermal delivery [44].

2.4.4 Drug Delivery and Pharmaceutical Composition

Delivery of drug/pharmaceuticals to patients in the most physiologically acceptable manner has always been an important concern in medicine. In general, the smaller the dimensions of the drug and the coating material required to encapsulate the drug, the better the drug to be absorbed by human being. Drug delivery with polymer nanofibers is based on the principle that dissolution rate of a particulate drug increases with increasing surface area of both the drug and the corresponding carrier if needed. As the drug and carrier materials can be mixed together for electrospinning of nanofibers, the likely modes of the drug in the resulting nano structured products are: (1) drug as particles attached to the surface of the carrier which is in the form of nanofibers, (2) both drug and carrier are nanofiber-form, hence the end product will be the two kinds of nanofibers interlaced together, (3) the blend of drug and carrier materials integrated into one kind of fibers containing both components, and (4) the carrier material is electrospun into a tubular form in which the drug particles are encapsulated. The modes (3) and (4) are preferred. However, as the drug delivery in the form of nanofibers is still in the early stage exploration, a real delivery mode after production and efficiency have yet to be determined in the future [44].

2.4.5 Filtration

Polymeric nanofibers have been used in air filtration applications for more than a decade [45]. Due to poor mechanical properties of thin nanowebs, they were laid over a substrate suitable enough to be made into a filtration medium. The small fiber diameters cause slip flow at fiber surfaces, causing an increase in the interception and inertial impaction

efficiencies of these composite filter media [46]. The enhanced filtration efficiency at the same pressure drop is possible with fibers having diameters less than 0.5 micron [46].

The potential for using nanofiber webs as a filtering medium is highly promising. Knowing that the essential properties of protective clothing are high moisture vapor transport, increased fabric breathability, and enhanced toxic chemical resistance, electrospun nanofiber membranes have been found to be good candidates for these applications [47]. The highly porous electrospun membrane surfaces help in moisture vapor transmission. Gibson et al. have analyzed the possibility of using thin nanofiber layers over the conventionally used nonwoven filtration media for protective clothing [48]. Polyurethane and nylon nanowebs were applied over open cell foams and carbon beads and tested for air flow resistance. They concluded that the airflow resistance, filtration efficiency, and pore sizes of nonwoven filter media could be easily altered by coating with the lightweight electrospun nanofibers [48]. Doshi et al. have evaluated composites of nanofibers with spunbond and melt blown fabrics for filtration characteristics [49]. The nanofiber composite membranes have shown very high increase in the filtration efficiencies [49]. Researchers at General Motors Company are working on nanofibers for different composite applications because of its scratch/ wear resistance, low temperature ductility, low flammability, and recyclability [50].

Nanofibers also find applications in aerospace and semiconductor industries. Piezoelectric polymers were electrospun and investigated for applicability as a component on the wings of micro-air vehicles [51].

2.5 Characterization of Nanofibers

Although the concept the electrospinning dates back to many years from now, not much of characterization has been done in this field. The demand of these electrospun fibers in wide variety of applications has influenced to develop the characterization and testing techniques for the nanofibers produced.

One of the foremost roles of the electrospinning process is to produce small diameter fibers. Almost everybody who has done electrospinning experiments has reported that the fibers spun through this process have fiber diameters in the range of a few nanometers to a couple of microns. Fibers spun through different polymer solutions did not make much of a difference in the fiber diameter. The measurement of fiber diameter in the electrospun webs that have been reported in the literature is based using various image analysis techniques. The instruments for measuring the fiber diameter and the analysis have been done using various instruments, mainly scanning electron microscope, transmission electron microscope and atomic force microscopes.

There is very little data available in the literature on the mechanical properties of electrospun nonwoven mats because not much work is done in this field [52]. It has been supposed that nanofibers can have better mechanical performance than microfibers [44]. Till now in the open literature no one has given information in detail regarding their mechanical properties and how the electrospinning process parameters affect their properties.

During the service lifetime of the nanofibers, forces exerted on the fibers in the form of mechanical contact or thermal misfit may result in permanent deformation or

even failure. Therefore, there is a need to characterize the mechanical properties of single nanofibers. Commercial mechanical testing systems have been used to test fibers as small as about 10 μm in diameter [53]. However, as the size of the fibers is further reduced, such mechanical testing systems are not suitable for testing these ultrafine fibers due to the following challenges:

1. Manipulating extremely small fibers. Due to the small size of the nanofibers, handling these fibers without damaging them can be very challenging. Custom made [54] and commercial [55] micro-manipulation systems can be used to move the fibers and attach the fiber ends to grips or fixtures. However, such systems may not be suitable for certain types of nanofibers as will be explained next.

2. Finding suitable mode of observation. Most of the manipulation systems are more suitable for operation under scanning electron microscopes (SEM) since the magnification of optical microscopes is insufficient for observing nanofibers in the lower nanometer range (<250 nm). This limits the use of the manipulation systems to conductive samples such as carbon nanotubes. Non-conductive samples such as polymers may be damaged by the electron beam in the SEM. Similarly, mechanical tests can be carried out in SEM [54] and transmission electron microscope (TEM) [56] for conductive samples only.

3. Sourcing for accurate and sensitive force transducer. The load resolution of most commercial mechanical testing systems depends on the type of load cell used. The smallest load cell of such systems can achieve a load resolution of 0.1 mN [57]. This resolution is insufficient for the testing of nanofibers since the force required to break them can be in the nano Newton range. One commercially available mechanical testing system that may now be suitable for nanofibers with diameters in the range of hundreds of nanometers is the NanoBionix (MTS, USA). It has a load resolution of 50 nN.

4. Sourcing for accurate actuator with high resolution. The lengths of nanofibers can range from a few micrometers for nanowires to a few centimeters for continuous electrospun fibers. An actuator with high resolution is especially crucial for short fibers since the fibers can break in less than one micrometer of deformation [58, 59].

5. Preparing samples of single-strand nanofibers. Single strand nanofibers have to be prepared in order to obtain the mechanical properties of individual fibers. This may not be difficult if MEMS are used to stretch single strand samples since they can be prepared using conventional micro fabrication methods. However, if the nanofibers are fabricated in the form of a three-dimensional continuous network, isolating single fibers for mechanical tests can be difficult. One such example is a nanofibrous scaffold produced by the phase separation method [60].

A review of the mechanical characterization techniques has been developed to test nanofibers by E.P.S. Tan, C.T. Lim. These techniques include tensile test, bend test and indentation done at the nanoscale [7].

CHAPTER 3

RESEARCH OBJECTIVE

This thesis was divided into two parts because while working on part I in the process of making aligned nanofiber, it was observed that to obtain single nanofiber is challenging and if mechanical behavior of single nanofiber is indentified then it can be useful from various aspect of applications. This led to part II of thesis for which characterization technique was used to investigate mechanical properties.

The objective of first part of the thesis is to produce aligned nanofiber of poly L lactic acid using electrospinning and properly obtain that specimen of single nanofiber to study their mechanical behavior in biorelevant conditions.

The objective of second part of the thesis is to perform testing on single nanofiber to investigate mechanical properties of single nanofiber using scanning electron microscopy (SEM), atomic force microscopy (AFM).

CHAPTER 4

EXPERIMENTAL DESIGN

At the outset, this chapter gives a brief introduction about the description of the project and discusses the materials which are utilized in this research to produce nanofiber. It explains the methods that are used in this research to produce aligned nanofiber. This includes the apparatus design and the typical electrospinning conditions that are used to get the aligned nanofiber. Finally a brief description of the characterization procedure using Scanning Electron Microscopy (SEM) and Atomic Force Microscopy (AFM) is given.

The mechanical properties of nanofibrous scaffold can affect cell morphology, proliferation. In order to evaluate the mechanical behavior of scaffolds under various loading conditions, it is necessary to obtain the mechanical properties of individual fibers that make up the scaffold. So in order to use the fabricated nanofibers for mechanical tests, an appropriate method is required for isolating and handling single nanofiber filament. In order to meet the above requirements, the electrospinning apparatus was designed to guide the electrospinning jet, which made possible to collect the electrospun nanofiber as uniaxially aligned arrays.

4.1 Electrospinning Equipment

To achieve the research objectives, an electrospinning apparatus setup was designed and constructed. The apparatus consists of two main devices, the sprayer and the collecting device.

The spraying setup (Figure 4.1) has a syringe fitted with a needle. The polymer solution to be electrospun was loaded into the syringe. A constant flow rate of 3.5ml/hr was maintained using the syringe pump. The positive output lead of a high voltage power supply (Gamma High Voltage Power Supply ES30P; Gamma High Voltage Research, Ormond Beach, FL), set to 20 kV, was attached to a 20 gauge (inner diameter 0.023") needle on the syringe. The 20-gauge needle was used for making nanofibers.

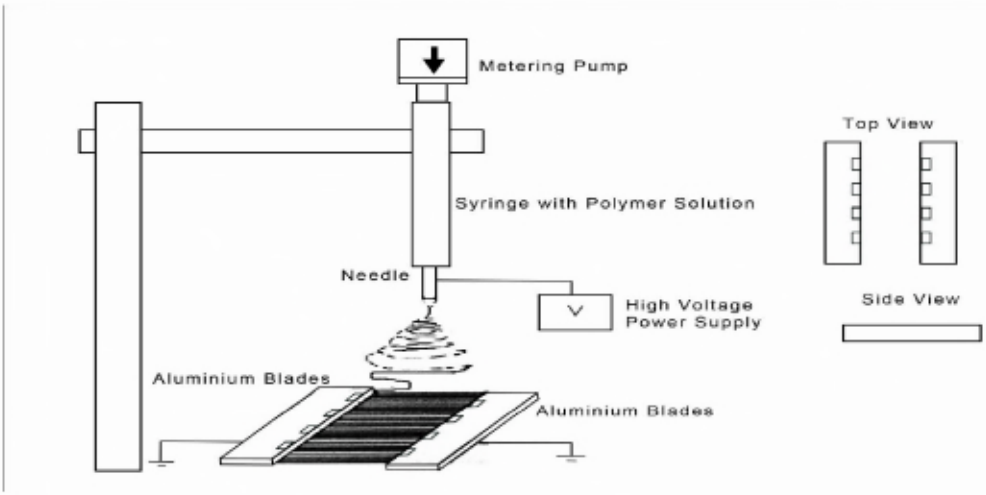

Figure 4.1 Diagrammatic representation of electrospinning equipment.

Electrical sparks were observed if a small metal part was around the system. As the process needs voltage of very high order, proper care must be taken in understanding the electrical connections of the system. A detailed version of the chemical and electrical safety factors is listed in Appendix A.

The electrospinning process is affected by varying the electric potential, flow rate, concentration, distance between the capillary and collection screen, size of the needle, and also by the ambient parameters such as temperature and humidity.

The two variables considered for this work were the concentration of the polymer in the solution, and the diameter of the needle. The needle used was 20-gauge distance,

wherein electric voltage is the applied voltage to the polymer solution and collecting distance. The voltage used for the process was 20 kV. The collector to needle distance was 20 centimeters. For the fabrication of PLLA nanofibers, a 20-gauge needle was used for spinning a solution of 5% w/w, 6% w/w concentration. After this, in order to assess the mechanical properties of electrospun fibers, a single filament of nanofiber was obtained with the technique of double sided tape suck on parallel plates which allows single nanofiber to be isolated and handled. A method has been developed to isolate individual electrospun fibers. The parallel arrangement of aluminum electrodes with a double sided tape was attached to both the ends of the aluminum electrodes to facilitate the attachment of fibers. The distance between the parallel strips was set to 1.2 cm to accommodate the height of the frame.

The fibers were electrospun with a typical flow rate of 3.5 ml/hr and a potential difference of 20 kV was applied. Electrospun process was carried out only for a few seconds to get a few strands of fibers across the aluminum electrodes. Individual fibers were sited and isolated in the spaces formed by the parallel strips. By easily removing the double sided tape from aluminum electrodes, the single fiber could be handled.

4.2 Materials

Electrospinning experiments were carried out using Poly-L-lactide, Resomer® L207 [Boehringer Ingelheim Fine Chemicals]. Poly-L-lactide is a biocompatible and biodegradable polymer that makes it an ideal candidate for tissue engineering. Poly-L-lactide has been used in medical applications, such as biodegradable sutures, since the 1960s. PLA exists as L-PLA (mainly crystalline) or DL-PLA (mainly amorphous).

Through the manipulation of the co-polymer characteristics (such as the interconnectivity of the internal 3-D geometry, mechanical and structural integrity, and biodegradability) these scaffold structures can be designed and fabricated to suit a particular tissue engineering application.

The solvent used for preparing a solution of Poly-L-lactide was Methylene Chloride (Fisher Scientific). Resorbable polymeric biomaterials are traditionally processed in organic solvents such as methylene chloride. Potential advantages of the use of organic solvents in tissue engineering applications are that they can prevent hydrolysis of substrates/products and their use may allow a better integration with chemical steps/processes.

4.3 Solution Preparation

The solutions of Poly-L-lactide were prepared in glassware using the following technique. Glassware was cleaned using an initial rinsing with tap water. The desired amount of Poly-L-lactide, according to the concentration required was weighed. These polymer chips were poured into a glass bottle containing a measured amount of methylene chloride. The glass bottle was closed with an airtight lid to maintain the concentration throughout. A homogeneous solution was achieved by slow agitation. Agitation was done by using a magnetic stirrer. The agitation was slow to avoid mechanical degradation of the polymer chains. All solutions were prepared at room temperature.

A solution concentration of 5% w/w was achieved by dissolving 10 grams of PLLA in 190 grams of Methylene Chloride. This concentration was used for electrospinning nanofiber.

4.4 Characterization of Electro-spun Nanofibers

The electrospun aligned nanofibers were characterized based on morphology, and mechanical properties. The morphology of the nanofiber was studied using SEM, mechanical properties of nanofiber was studied using AFM. The following sections describe the methods implemented to measure the morphology, and mechanical properties of the nanofiber produced for this study.

4.4.1 Morphology

Understanding how the morphology is affected by solute used is essential to produce fibers with desired properties. Images of nanofibers were captured by scanning electron microscopy (SEM) as a first step to determine fiber diameter and distribution. Electrospinning process produces very fine fibers down to a few nanometers. The scanning electron microscope (SEM) has many advantages over optical microscopes. The SEM has a large depth of field, which allows more of a specimen to be in focus at one time. The SEM also has much higher resolution; so closely spaced specimens can be magnified at much higher levels. Because the SEM uses electromagnets rather than lenses, the researcher has much more control in the degree of magnification. All of these advantages, as well as the actual strikingly clear images, make the scanning electron microscope one of the most useful instruments in characterizing the nanofibers produced by electrospinning.

The SEM is an instrument that produces a largely magnified image by using electrons instead of light to form an image. A beam of electrons is produced at the top of the microscope by an electron gun. The electron beam follows a vertical path through the microscope, which is held within a vacuum. The beam travels through electromagnetic fields and lenses, which focus the beam down toward the sample (Figure 4.2).

Once the beam hits the sample, electrons and X-rays are ejected from the sample. Detectors collect these X-rays, backscattered electrons, and secondary electrons and convert them into a signal that is sent to a screen similar to a television screen. This produces the final image.

Because the SEM utilizes vacuum conditions and uses electrons to form an image, special preparations must be done to the sample. All water must be removed from the samples because the water would vaporize in the vacuum. All metals are conductive and require no preparation before being used. All non-metals need to be made conductive by covering the sample with a thin layer of conductive material.

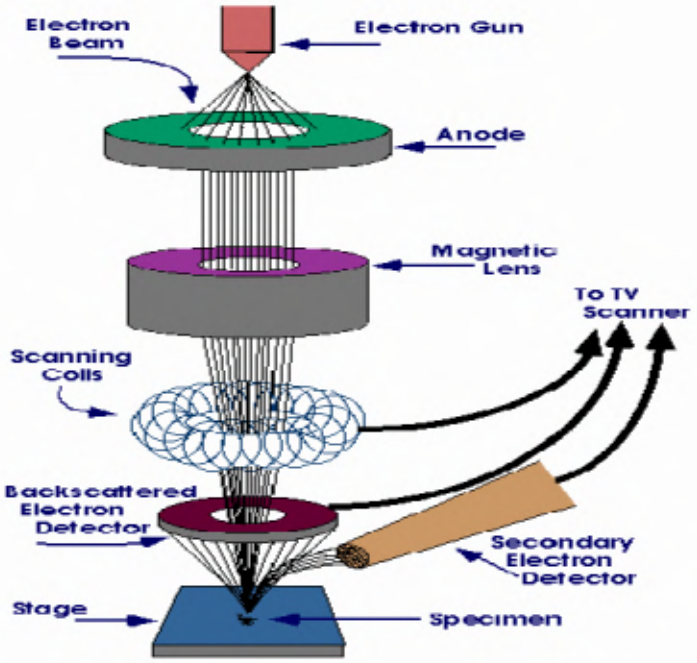

Figure 4.2 Schematic of the Operation of a SEM. (Diagram courtesy of Iowa State University)

The electrospun samples need no preparation, as they are electrically conductive. The samples were prepared by directly removing the double sided tape from the aluminum plates on which aligned fibers were deposited. The stub has an area of around 120 square

millimeters, so the specimen samples were stuck in such a way that 4 to 5 could fit into the stub. A layer of carbon tape (double sided) is pasted to the stubs and the sample is stuck to the other side of the tape. Carbon tapes are used to prevent the charging of the sample. Carbon tapes dissipate the excessive charge buildup. The specimen fixed stubs was then mounted on the microscope chamber. To begin with the image capturing, proper spot size and accelerating voltage should be selected. Higher accelerating voltage will increase resolution, but also increases specimen damage, contamination, and charging, and decreases surface detail.

Therefore, a voltage of 1 kV was used for all the samples. After setting the voltage, the samples were magnified to the desired size. The processes of stigmation, apertures align and focus was repeated for proper black level and gain level for clarity and was digitally scanned and stored. The SEM used for the study was Leo 1530VP.

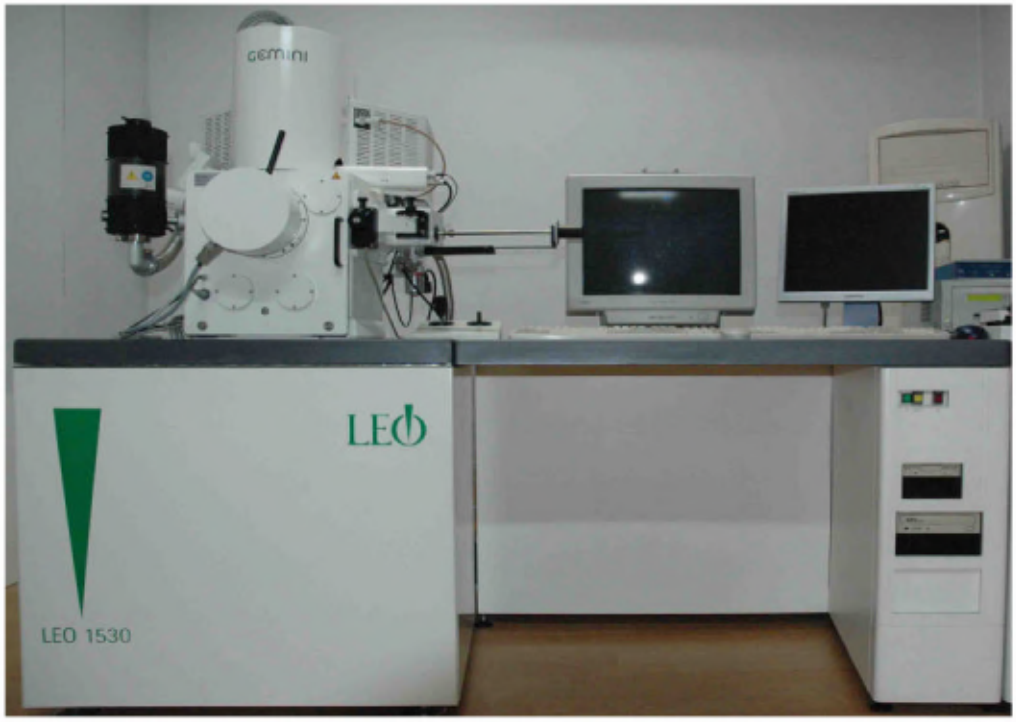

Figure 4.3 LEO 1530 Field Emission SEM

The analyses of the electrospun nanofibers were done with the help of LEO 1530 Field Emission SEM (Figure 4.3). The LEO 1530 is an ultra-high resolution field emission SEM utilizing the GEMINI field emission column. It is well suited to a wide range of applications due to its versatile specimen chamber and eucentric stage. Six free ports for the attachment of optional detectors and accessories enable the instrument to be used as a complete analytical workstation.

The electrospun nanofibers samples used in this method were coated. The SEM was interfaced with computer having LEO 320 software. Since the scanning electron microscope uses a high voltage for its operation and the electron beam is so sharp and intense that a small speck of dust in the system or in the sample may ruin the measurement of the whole sample. So proper care must be taken while preparing the sample and mounting the sample on the microscope.

4.5 Mechanical Properties

The atomic force microscope (AFM) can image the three-dimensional structure of nanofibers in a physiological environment enabling real-time biochemical and physiological processes to be monitored at a resolution similar to that obtained for the electron microscope (EM). The process of image acquisition with the AFM probe allows forces to be measured at the molecular level [61]. Indentation of Nano-materials with the AFM tip provides detailed micromechanical properties. The indentation method existed prior to the development of the AFM and is a convenient test to assess the mechanical properties.

4.5.1 AFM Development & Principle of Operation

The atomic force microscope (AFM) or scanning force microscope (SFM) was invented in 1986 by Binnig, Quate and Gerber [62]. Similar to other scanning probe microscopes, the AFM raster scans a sharp probe over the surface of a sample and measures the changes in force between the probe tip and the sample. Figure 4.4 illustrates the working concept for an atomic force microscope. A cantilever with a sharp tip is positioned above a surface. Depending on this separation distance, long range or short range forces will dominate the interaction. This force is measured by the bending of the cantilever by an optical lever technique: a laser beam is focused on the back of a cantilever and reflected into a photodetector. Small forces between the tip and sample will cause less deflection than large forces. By raster-scanning the tip across the surface and recording the change in force as a function of position, a map of surface topography and other properties can be generated [63, 64, 65].

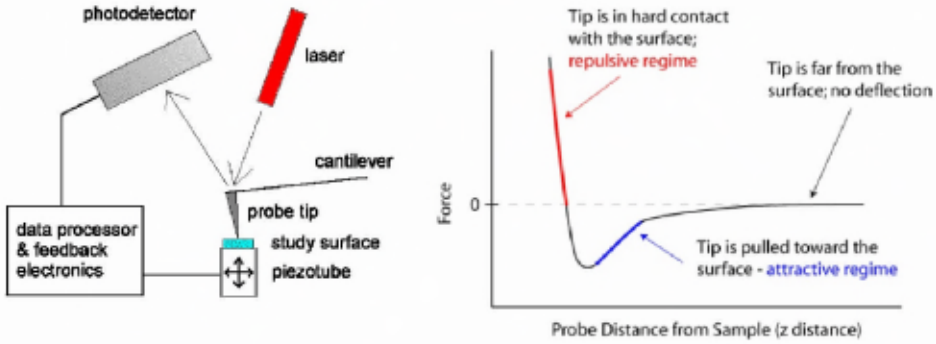

Figure 4.4 Scheme of an atomic force microscope and the force-distance curve characteristic of the interaction between the tip and sample [62].

The AFM is useful for obtaining three-dimensional topographic information of insulating and conducting structures with lateral resolution down to 1.5 nm and vertical resolution down to 0.05 nm. These samples include clusters of atoms and molecules, individual macromolecules, and biologic al species (cells, DNA, proteins). Unlike the

preparation of samples for STM imaging, there is minimal sample preparation involved for AFM imaging. Similar to STM operation, the AFM can operate in gas, ambient, and fluid environments and can measure physical properties including elasticity, adhesion, hardness, friction and chemical functionality [63, 64, 65].

Basic set-up of an AFM

In principle the AFM resembles a record player and a stylus profilometer. The ability of an AFM to achieve near atomic scale resolution depends on the three essential components: (1) a cantilever with a sharp tip, (2) a scanner that controls the *x*-*y*-*z* position, and (3) the feedback control and loop.

1. *Cantilever with a sharp tip.* The stiffness of the cantilever needs to be less the effective spring constant holding atoms together, which is on the order of 1 - 10 nN/nm. The tip should have a radius of curvature less than 20-50 nm (smaller is better) a cone angle between 10-20 degrees.

2. *Scanner.* The movement of the tip or sample in the *x*, *y*, and *z*-directions is controlled by a piezo-electric tube scanner, similar to those used in STM. For typical AFM scanners, the maximum ranges are 80 µm x 80 µm in the *x*-*y* plane and 5 µm for the *z*-direction.

3. *Feedback control.* The forces that are exerted between the tip and the sample are measured by the amount of bending (or deflection) of the cantilever. By calculating the difference signal in the photodiode quadrants, the amount of deflection [(A+B)-(C+D)] can be correlated with a height (Figure 4.5). Because the cantilever obeys Hooke's Law for small displacements, the interaction force between the tip and the sample can be determined.

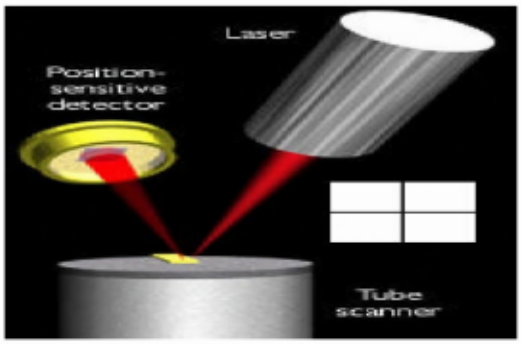

Figure 4.5 Schematic diagram of optical changes in the deflection of the cantilever and a quadrant photodiode [62].

The AFM can be operated with or without feedback control. If the electronic feedback is **on**, as the tip is raster-scanned across the surface, the piezo will adjust the tip-sample separation so that a constant deflection is maintained—or so the force is the same as its setpoint value. This operation is known as *constant force mode*, and usually results in a fairly faithful topographical (hence the alternative name, *height mode*).

If the feedback electronics are switched **off**, then the microscope is said to be operating in *constant height* or *deflection* mode. This is particularly useful for imaging very flat samples at high resolution. Strictly, this mode should then be called *error signal*. The error signal may also be displayed while the feedback is on; this image displays slow variations in topography and highlights the edges of features [63, 64].

4.5.2 Modes of operation for the AFM

The three general types of AFM imaging are contact mode, tapping mode and non-contact mode [63, 64].

Contact mode

Contact mode is the most common method of operation of the AFM and is useful for obtaining 3D topographical information on nanostructures and surfaces. "Contact" represents the repulsive regime of the inter- molecular force curve, the part of the curve above the x-axis (Figure 4.6, right image). Most cantilevers have spring constants < 1 Nm, which is less than effective spring constant holding atoms together.

Figure 4.6 Scheme of contact mode imaging and an image of cholera oligomers [63].

One of the drawbacks of the tip remaining in contact with the sample is that large lateral forces can be exerted on the sample as the tip is dragged over the specimen. These large forces can result in deformed images and damaged samples. Small lateral forces, however, can be used to provide information on the friction (drag resistance) between the tip and sample in a mode known as *lateral force microscopy* (LFM).

LFM measures the torsional deformation of the cantilever while the tip scans over the surface. While topographic images are recorded by the difference between the top and bottom quadrants of the photodiode, the frictional images are recorded by the difference between the left and right portions of the photodiode. Simultaneous measurement of the topographic and frictional images can be recorded. LFM is useful for obtaining chemical contrast in samples whose features are all of the same height.

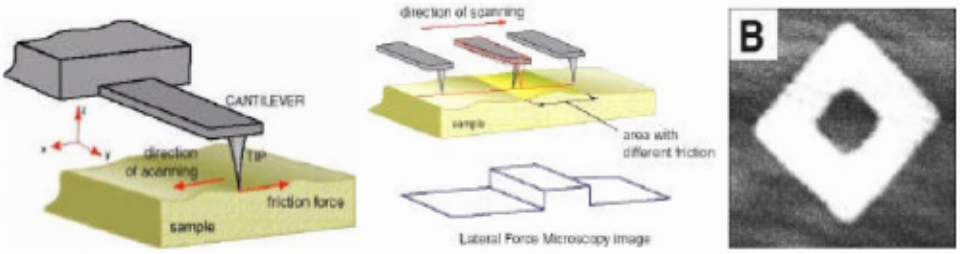

Figure 4.7 Scheme of lateral force imaging and a friction image of self-assembled monolayers on gold. The white regions terminate in –COOH, and the gray regions terminate in $–CH_3$; the tip is also functionalized with –COOH [63].

Tapping mode

Tapping mode is another mode of operation for AFM. Unlike the operation of contact mode, where the tip is in constant contact with the surface, in tapping mode the tip makes intermittent contact with the surface. As the tip is scanned over the surface, the cantilever is driven at its resonant frequency (hundreds of kHz). Because the contact time is a small fraction of its oscillation period, the lateral forces are reduced dramatically.

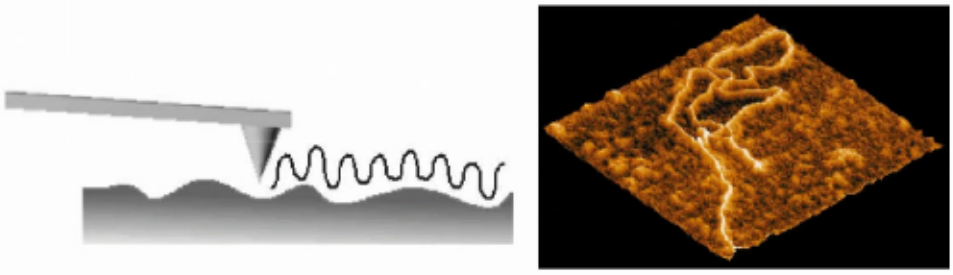

Figure 4.8 Scheme of Tapping mode imaging and an image of DNA [64].

Tapping mode is usually preferred to image samples with structures that are weakly bound to the surface or samples that are soft (polymers, thin films). There are also two other types of image contrast mechanisms in tapping mode:

Amplitude imaging. The feedback loop adjusts the *z*-piezo so that the amplitude of the cantilever oscillation remains (nearly) constant. The voltages needed to keep the amplitude constant can be compiled into an (error signal) image, and this imaging can often provide high contrast between features on the surface.

*Phase imaging***.** The phase difference between the driven oscillations of the cantilever and the measured oscillations can be attributed to different material properties. For example, the relative amount of phase lag between the freely oscillating cantilever and the detected signal can provide qualitative information about the differences in chemical composition, adhesion, and friction properties.

Non-contact mode is a method where the cantilever is oscillated above the surface of the sample at distance such that it is no longer in the repulsive regime but in the attractive regime of the inter- molecular force curve. The operation of non-contact imaging is quite difficult in ambient conditions because of the existing thin layer of water on the tip and the surface. As the tip is brought close to the surface, a small capillary bridge between the tip and the sample and cause the tip to "jump-to-contact."

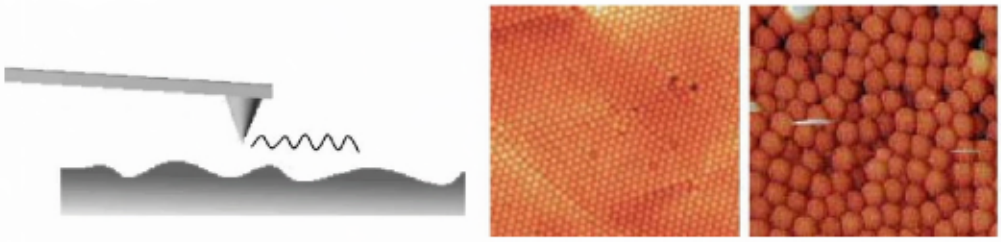

Figure 4.9 Scheme of non-contact mode imaging and an image of raspberry" polymers, DI

The choice for which AFM mode to use is based on the surface characteristics of interest and on the hardness/stickiness of the sample. Contact mode is most useful for hard surfaces; a tip in contact with a surface, however, is subject to contamination from removable material on the surface. Excessive force in contact mode can also damage the surface or blunt the probe tip. Tapping mode is well-suited for imaging soft biological specimen and for samples with poor surface adhesion (DNA and carbon nanotubes). Non-contact mode is another useful mode for imaging soft surfaces, but its sensitivity to external vibrations and the inherent water layer on samples in ambient conditions often causes problems in the engagement and retraction of the tip [63, 64].

4.5.2 Atomic Force Microscope Operation

The AFM probes the surface of a sample with a sharp tip, a couple of microns long and often less than 100 A^0 in diameter. The tip is located at the free end of a cantilever that is 100 to 200 micrometer long. Forces between the tip and the sample surface cause the cantilever to bend, or deflect. A detector measures the cantilever deflection as the sample is scanned under the tip. The measured cantilever deflections allow a computer to generate a map of surface topography as shown in the Figure 4.10.

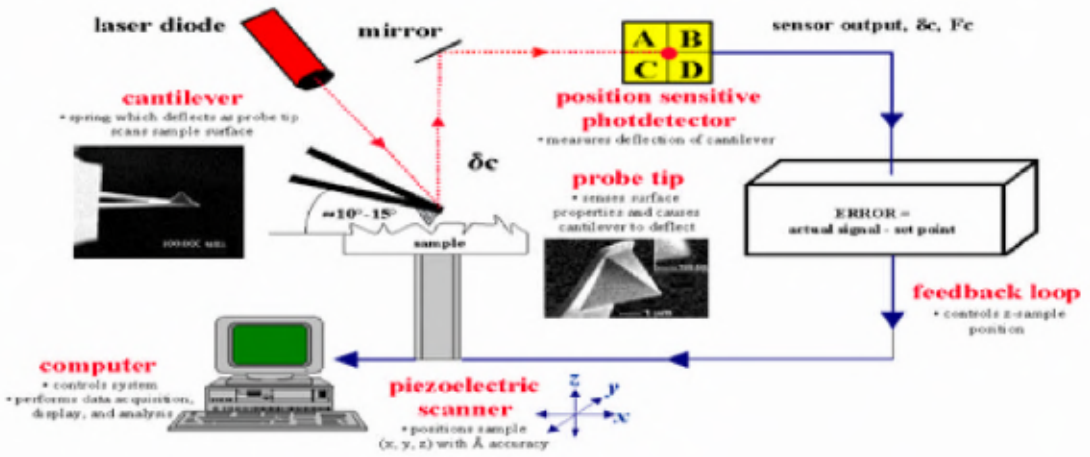

Figure 4.10 Atomic Force Microscope schematic Diagram with components [99].

4.5.3 Forces Affecting AFM Probe

The sum of the forces on the tip causes the deflection of the cantilever; these forces can be attractive or repulsive. The forces acting on the tip vary depending on the mode of operation and the conditions used for imaging. In contact mode imaging, the tip is deflected, mainly due to repulsive forces from the overlapping electron orbitals between the tip atoms and the sample atoms. The dominant attractive force is a van der Waals force resulting primarily from the nonlocalized dipole-dipole interactions among atoms of the tip and specimen [62, 65]. While imaging in fluids contributions from electrostatic Coulomb interactions between charges on the specimen and tip (either occurring naturally or induced because of polarization), osmotic pressure due to charge movements and rearrangements, and structural forces such as hydration force, solvation force, and adhesion force should be considered [67]. The manner in which the AFM generates images also makes it an excellent sensor of molecular forces (hydrogen bonds, van der Waals and electrostatic forces). In tapping mode imaging, due to the interaction of forces acting on

the cantilever when the tip comes close to the surface, Van der Waals force, dipole-dipole interaction, electrostatic forces, etc. cause the amplitude of this oscillation to decrease as the tip gets closer to the sample. An electronic servo uses the piezoelectric actuator to control the height of the cantilever above the sample. The servo adjusts the height to maintain a set cantilever oscillation amplitude as the cantilever is scanned over the sample. A tapping *AFM* image is therefore produced by imaging the force of the intermittent contacts of the tip with the sample surface [68, 69].

4.5.4 Measuring the Elastic Properties with the AFM

Other methods have been used to measure the elastic properties are flicker spectroscopy [70], and optical tweezers [71, 72]. Bereiter-Hahn and coworkers used another scanning microscopy technique, scanning acoustic microscopy, to measure the elastic properties of cells locally [73, 74]. The main difference between AFM and these techniques is the high lateral resolution (100 nm) provided by the AFM with the potential to increase with improved tip design [75].

AFM data can be interpreted as elasticity measurements [76-79]. The AFM allows the mechanical properties of fibers to be determined accurately from force-versus-distance curves (force curves) [80, 81]. The relationship between indentation force and depth depends upon the tip geometry and the mechanical properties of the specimen [82].

If the sample is soft, the tip will deform it, and elastic indentation occurs. The force versus indentation curves becomes non-linear for softer samples, because the compliance of the sample becomes higher for larger loading forces. Radmacher considers the geometry of AFM tips to be conical, on a scale of several 10's to 100s of nm [75]. The contact area of the probe increases with indentation, the force-depth relationship in any soft material is

nonlinear, making it difficult to assess how much of the response is due to the tip geometry [82]. Since, the contact area will increase while loading, indenting the sample. This process has been treated analytically by Hertz, where a relationship between the indentation and the loading force is given for smooth parabolic indenter profiles [83]. Most investigators have attributed nonlinearity of the indentation response entirely to the tip geometry, and have applied equations based on classical infinitesimal strain theory to extract the Young's modulus (E) of the material [84, 85].

4.5.5 Assumptions and Challenges

There are many assumptions that must hold for an accurate modulus determination with the Hertz model, including that the material is linear elastic, homogeneous, and infinitely thick, with no adhesion or attraction between the tip and the sample. Care must be taken to ensure that the sample in question can be described within these assumptions or that the deviations from these assumptions are considered. Although most biological materials have viscoelastic properties, at the indentation rates (2 μm/s) and depths (<100 nm) typically used in AFM nanoindentation, the force curves can be consistent with a linear elastic material and an elastic modulus can be defined. If the force curves show any indication of viscoelasticity (hysteresis in the loading and unloading curves in the force curve) or sample adhesion, it may not be appropriate to use the Hertz model or to define an elastic modulus. The range of indentation depths that can be accurately modeled is also dependent on the sample thickness. For soft or thin samples (and larger indentation depths), the influence of the substrate on the measured elastic modulus must be considered. The elastic modulus can be plotted as a function of indentation depth, and it can be verified that the elastic modulus is independent of indentation depth for at least small indentation depths. An increase in modulus with indentation depth may be indicative of an increasing

contribution from the substrate. It is also important to note that the AFM measures the modulus at the surface of the material and may be more accurately termed local modulus. Measuring a local modulus can be advantageous for certain experiments. For example, this allows a determination of the substrate elastic modulus a cell would sense on the surface of the substrate. Additionally, any heterogeneity in modulus across the substrate can be observed by obtaining a force map. It should also be noted that with the AFM, the modulus is measured in compression as the AFM tip is indented into the sample surface. The modulus measured with AFM may, therefore, be different from that obtained from other techniques, such as tensile testing, because of the differences in the direction of applied strain and any anisotropy of the sample. In addition, tensile testing measures the modulus of the sample in its entirety, whereas the AFM will be sensitive to changes in the mechanical properties between the surface and the bulk.

The Hertz equation also requires accurate knowledge of the initial contact point of the tip with the sample. This value can be difficult to determine from the force curves, particularly when there is tip-sample attraction or there is water or a contamination layer on the sample surface that the tip senses before it comes in contact with the surface. The Hertz equation can be fitted to the experimental data with two unknowns in the equation, fitting for both E and Zo, the initial contact point. This eliminates the need to choose the value of Zo manually. The user must still be aware that changes in the value of Zo can significantly affect the calculated modulus value.

Accurate determination of the elastic modulus requires accurate calibration of the system, including the scanner and the cantilever. Calibration of the scanner must be checked periodically with an appropriate calibration grid for the size of the scanner. Each cantilever must also be calibrated so that the deflection sensitivity and the spring constant

are known. The deflection sensitivity (nm/V) is found by taking a force curve on a hard surface, with no indentation into the surface. In this case d = z, and the sensitivity is the slope of the deflection (d) versus z force curve. The deflection sensitivity must be calculated each time the laser is realigned on the cantilever. The spring constant must also be determined for each cantilever because the actual value may vary significantly from the nominal value provided by the manufacturer. There are several techniques that have been used to measure spring constants [86-96].

The advantages and disadvantages of each available method have been reviewed by Clifford and Seah [97]. Two popular methods are the Sader method, an equation that relates the spring constant to the length and width of the cantilever and the cantilever's resonant frequency, and the thermal tune method, which measures the cantilever's response to thermal noise. [91, 93-95]. In some instruments, the thermal tune method has been incorporated into the instrument hardware and software.

4.5.6 Tip and Cantilever Selection and Tip Functionalization

Proper choice of both cantilever stiffness and geometry of the incorporated tip are necessary for successful application of the AFM. Commercially available cantilevers have spring constants ranging from 0.006 N/m to 200 N/m. The spring constant used in our case was 0.041nN/nm, which was given by the manufacturer Brukers AFM. To avoid surface damage of nanofiber samples, imaging in contact mode and tapping mode, in either air or fluid, requires cantilevers with low spring constants, typically < 0.2 N/m. As mentioned previously, tapping mode is more generally used when imaging soft, biological samples. A low spring constant cantilever is also used for tapping mode in fluid, whereas a stiffer cantilever (typically approximately 45 N/m) is needed for tapping mode in air to reduce

noise. Low spring constant cantilevers also provide better deflection resolution, with a larger deflection for a given force, necessary for measuring intermolecular interactions, which typically range from 10^{-12} N to 10^{-7} N. The tip can be functionalized with molecules, proteins, or cells and the interactions of these tips with a surface of interest can be obtained. Several reviews are available describing these types of experiments [98].

AFM cantilevers with varying tip shapes are available. The standard geometry is of an integrated pyramidal tip with an end radius of 20 to 30 nm; sharper tips are also available. Radius of the tip for our probe was 15 nm, which was given by the manufacturer Brukers AFM. Sharper tips have the advantage of producing images with higher resolution. Sharper tips, however, have been shown to quickly deteriorate during scanning of cells, most likely because of tip contamination and blunting. Additionally, sharper tips have been associated with inducing increased damage to the cell surface.

CHAPTER 5

RESULTS

5.1 Morphology of Electrospun Nanofiber

The electrospun fibers were characterized with the scanning electron microscope for fiber diameter. The PLLA fibers were electrospun at a voltage of 20 kv, a collector to needle distance of 21 centimeters and a solution concentration of 5% w/w and 6% w/w. The needle used was a 20 gauge and the flow rate was 3.5 ml/hr. The PLLA fibers were in the size range of 150 nm to 800 nm (Figures 5.1, 5.2, 5.3, 5.4).

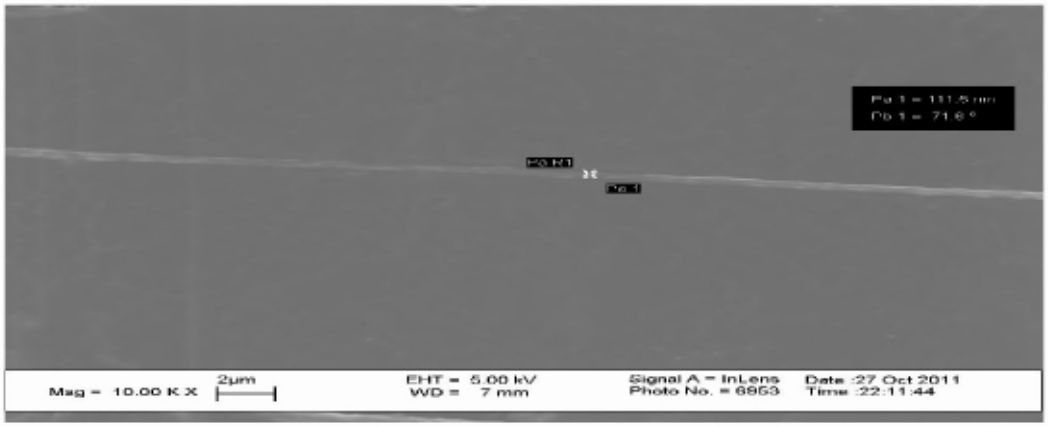

Figure 5.1 SEM Image of Single Nanofiber obtained with 5% polymer concentration

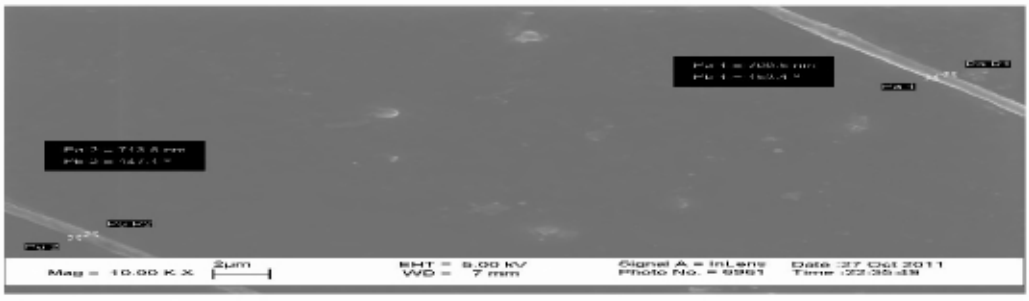

Figure 5.2 SEM Image of Parallel Aligned Nanofiber obtained with 6% polymer concentration

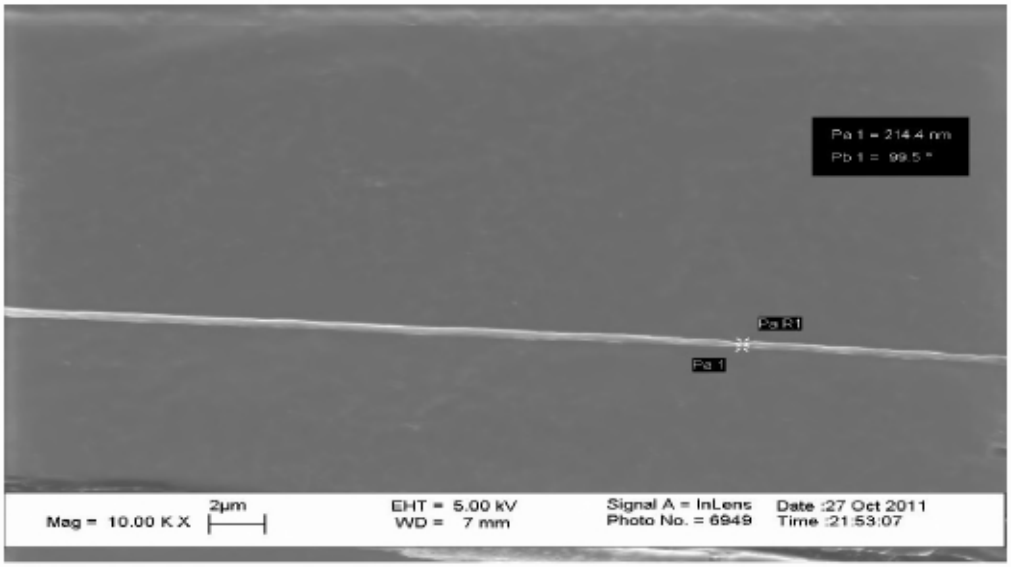

Figure 5.3 SEM Image of Aligned Nanofiber obtained with 6% polymer concentration

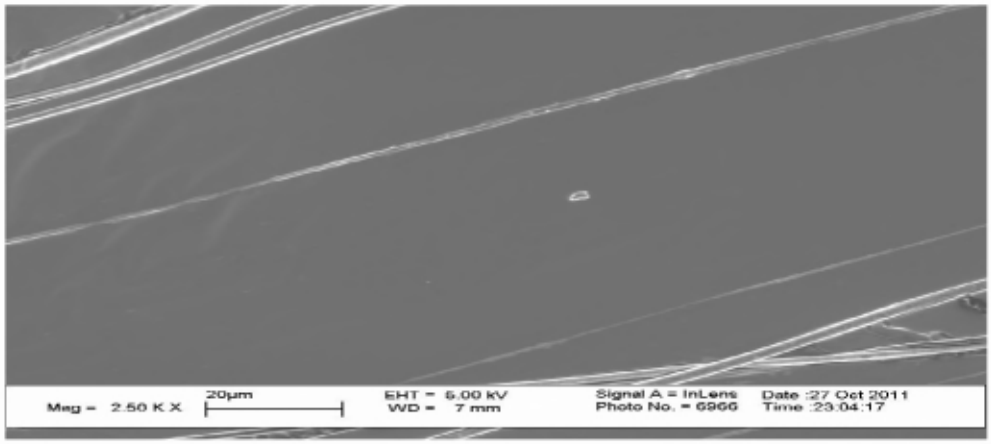

Figure 5.4: SEM Image of Aligned Fiber obtained with 5% polymer concentration

The range of the diameter size of the nanofiber is determined by measuring the least and highest diameter of the fiber from the SEM image. The least possible concentration, which would form a good nanofiber, was 5% and 6%. The SEM picture of single nanofiber of PLLA is shown in Figures 5.1, 5.3. The fiber diameter approximately ranged from 100 nm to 800 nm with most of them being in nanoscale. From SEM images it can be seen that most of the fibers are aligned straight.

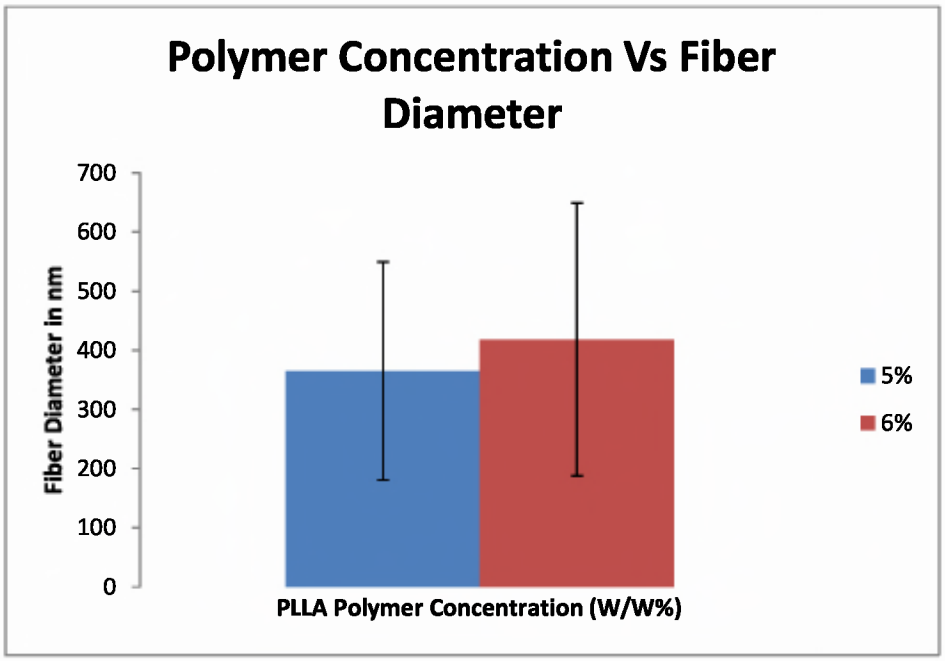

Figure 5.5: Bar Graph Representation of Polymer Concentration Vs Fiber Diameter.

The fiber diameter was obtained in nanoscale dimensions, by using the polymer concentration with 5% w/w, 6% w/w. The graph shows the standard deviation valves for both the concentration were in the 184.3 nm and 230.2 nm respectively and mean valve of both the concentration were 364.9 nm and 418.1 nm.

5.2 Mechanical Characterization of Electrospun Nanofibers

The AFM image of single nanofiber of PLLA is shown in Figures 5.6, 5.7. The left side image is tapping mode image where, the height of the nanofiber is visible. The right side image is phase image which is obtained with tapping mode image and phase shift signal is visible from the image. The brightness in the image shows, the amplitude is less and tip is in close contact with the sample. The contrast in the image shows, the amplitude is more

and is not in contact with the sample. This difference is because, the surface is rough and result which this image gives is the tip scan over the surface and based on the roughness of the surface, amplitude is changing with constant force maintained by feedback signal operating through computer software.

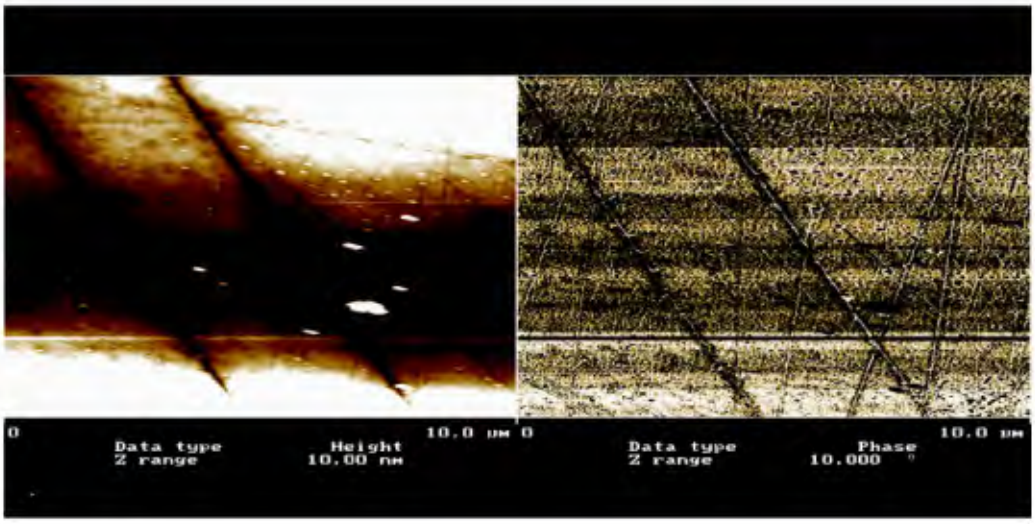

Figure 5.6: AFM Image of Parallel Aligned Nanofiber obtained with 5% polymer concentration

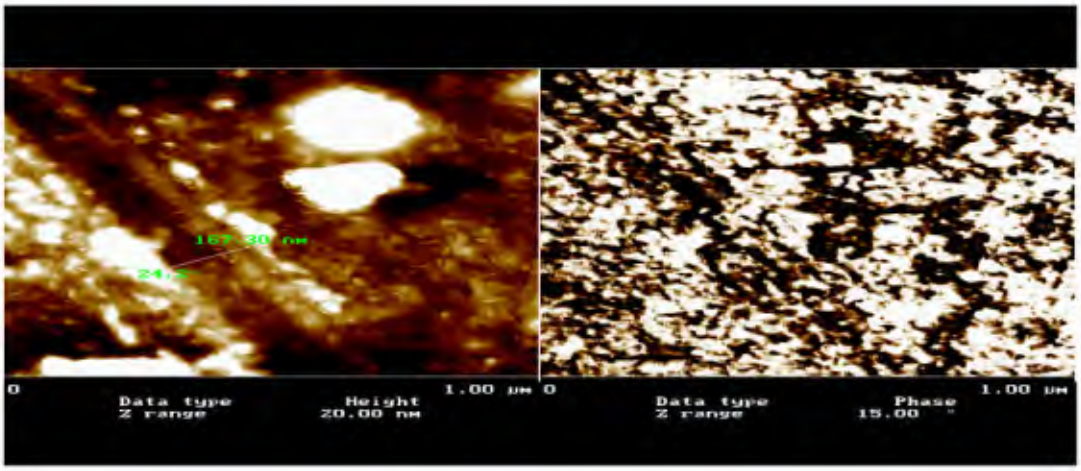

Figure 5.7: AFM Image of Single Nanofiber obtained with 5% polymer concentration

The image of nanofiber diameter obtained in tapping mode AFM is in range of 167 nm.

5.3 Force Calibration Plot

The force calibration plot obtained from the contact mode AFM. The force – distance curve would help to measure the Cantilever deflection, which would further determine the applied force on the sample. The cantilever deflection obtained from the calibration plot was 12.19 nm. The set point was set to 0 mV for accurate readings.

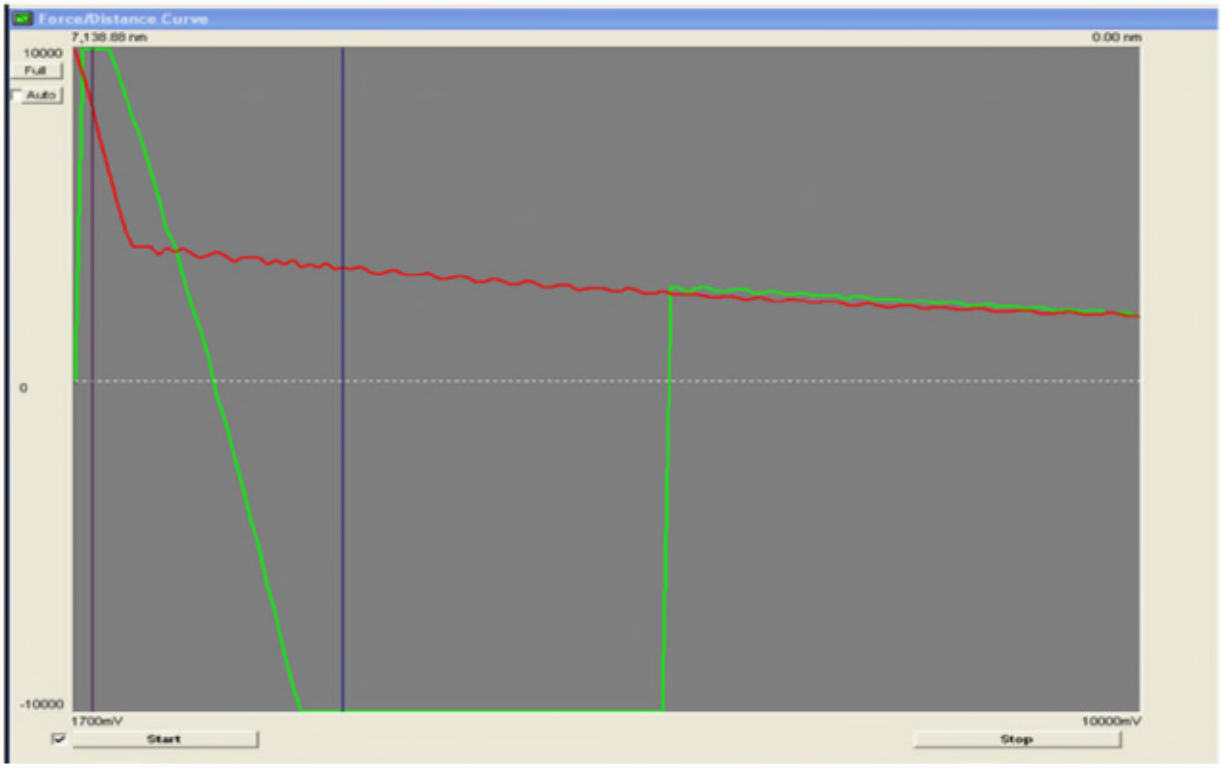

Figure 5.8: Force curve obtained from interaction between cantilever tip and the nanofiber sample.

The figure shows a typical force curve obtained from the interaction between cantilever tip and nanofiber. The z position of the cantilever is plotted on the x-axis and the cantilever deflection is plotted on the y-axis. Green line shows the tip sample interaction extending and red line shows the tip sample retracting. From the force curve diagram, it is well

understood that when the tip sample interaction is not there, the flat horizontal line. The moment the tip pulls downward, the attractive force is applied on tip and retraces back as the repulsive forces act on it. When the tip is no longer in contact with the sample, the force curve is again a horizontal line.

Any adhesion or interaction of the tip with the surface will be observed in the retraction force curve. The interaction force associated with this pull-off can be calculated using the equation of Hooke's Law:

Mathematically, Hooke's law states that

$$F=kx \tag{5.1}$$

where

x is the displacement of the spring's end from its equilibrium position (m);

F is the restoring force exerted by the spring on that end (N); and

k is a constant called the *rate* or *spring constant* (N/m).

Spring Constant for the cantilever probe is given by manufacturers which in this case is Brukers AFM probes = 0.041nN/nm.

x = Cantilever Deflection =?

x = Tip Deflection X Deflection Sensitivity

x = 199.99 mV X 0.061 mV/nm

X = 12.19 nm

Substituting these valves in Hooke's Law Equation (5.1):

$$= \frac{\cdot}{\quad} \times (\quad . \quad) \tag{5.2}$$

$$= . \tag{5.3}$$

Thus, the force applied on cantilever tip is 0.50 nN

Now to measure the Elastic Modulus E, Hertz Model was used.

The Hertz Model is given by

$$= \frac{\sqrt{\quad}}{\quad}(\quad) \quad / \tag{5.4}$$

$$= \quad - \tag{5.5}$$

F = Force on the probe = 0.50 nN

R = Radius of Probe = 15 nm.

v = Poisson's Ratio = 0.5 (for incompressible medium)

δ = Indentation into the surface of sample =?

δ = Z scanner displacement (Zs) – Cantilever Deflection (Zc).

$$= (\quad . \quad - \quad . \quad) \tag{5.6}$$

$$= \quad . \qquad < \quad = 15 \tag{5.7}$$

Means Hertz Model Equation fits to calculate the elasticity.

Elastic modulus was calibrated by substituting all the known valves in the Hertz model equation

$$= \frac{(. \times \quad \times \times \times . \ )}{(\times \quad . \times \quad)} \tag{5.8}$$

$$= \quad . \tag{5.9}$$

The force calibration plot allowed to find the force applied on the tip by satisfying Hooke's Law which was found to be 0.50 nN, which helped to find the elastic modulus = 22.9 MPa. The elastic modulus was calculated with the help of hertz model and was the local modulus calculated on the surface of the single nanofiber. The elastic modulus was calculated for 167 nm diameter nanofiber.

CHAPTER 6

DISCUSSION

The results show that the aligned nanofiber is the best way to study the characterization of single nanofiber, as it is easy to mount on stub of characterization technique to know about its morphology and mechanical properties. Here a unique approach was developed and used to handle and isolate the nanofiber by sticking double sided tape on aluminum plates arranged in parallel employed on electrospinning technique, which made possible to study the morphological and mechanical properties with ease as sample was properly mounted on stub. The alignment and fiber diameter in nanoscale dimensions was confirmed with the images obtained in Scanning Electron Microscope (SEM).

Atomic Force Microscope (AFM) was used to obtain the 3 dimensional image of nanofiber. Although AFM is not widely used in PLLA nanofiber research, many questions in polymer science can be addressed by use of this technique. The ability of the AFM to provide high-resolution images and to sense small forces in the sample's native environment make this technique invaluable in the characterization of nanofibers. Currently, the AFM has been used to determine the function of nanofiber made of PLLA with high-resolution imaging, to explore and quantify tip sample interactions, to characterize how nanoscale topography acts, to determine the mechanical properties of nanofiber in their native environment, and to help understand how a change in fiber diameter correlates with mechanical properties. The AFM can be used alone or can be combined with other optical and spectroscopic techniques to provide complementary information, creating an even more powerful tool. Also the person performing the

experimentation should be expert in handling AFM. Proper training is required to get the accurate results. The sharper you are in using AFM, the more well will be your results. Proper care should be care will mounting sample on AFM to avoid dust particles to settle down on stub. To have good judgment about the nanofiber in AFM, vast knowledge of AFM is necessary with at least 2 months of practice.

Calibration of force curve plot was done in Stevens Institute of Technology, as the software of multimode AFM in New Jersey Institute of Technology was not updated. The new version of software is required to obtain the results. The version currently used in New Jersey Institute of Technology is 4.4 3r5. As per the talk with technical support team of Brukers AFM Company, the new version can provide very good results with respect to both imaging and force calibration. The application of AFM will benefit evolving various other properties of nanofiber with application to polymer science. In this study, AFM was used to for measuring the force applied on the tip and also the elastic modulus of a nanofiber.

CHAPTER 7

CONCLUSIONS

The process of electrospinning was successfully carried out using PLLA as the polymer and methylene chloride as the solvent. By varying the concentration and the needle diameter, the process of electrospinning yielded very fine fibers with diameters in the nanometer range as well as fibers in the micron range. The nanofibers were selected for characterizing the mechanical properties using Scanning Electron Microscope and Atomic Force Microscope.

The electrospun nanofibers were cylindrical of varying diameters. The results of the SEM characterization showed that through electrospinning process, using PLLA 5% dissolving in methylene chloride as a solvent and maintaining flow rate of 3.5ml/hr, at 20 kV voltage, nanofibers in the range of 100 nm to 800 nm were obtained. The electrospun fibers had a good alignment with the help of parallel arrangement method used in electrospinning technique, which was favorable for mounting the sample for mechanical testing.

The AFM enabled us to image the three-dimensional structure of nanofiber allowing us to monitor its morphology and mechanical property. The tapping mode imaging and phase imaging was obtained and its morphological characteristic was observed. The force applied during the scanning was determined by using contact mode AFM, satisfying Hooke's Law, and was found to be 0.50 nN. To determine the mechanical properties of nanofiber, elasticity was measured with the help of Hertz Model and was obtained upto 22.9 MPa.

CHAPTER 8

FUTURE SCOPE OF RESEARCH

i. A study needs to be conducted to investigate how the diameter and distribution of diameter is affecting the mechanical properties of the aligned nanofiber.

ii. To obtain aligned nanofiber of different materials/polymer.

iii. Measure characterization and mechanical properties of different materials/polymer.

iv. Measure various other mechanical properties like tensile properties on single aligned nanofiber by innovating the mounting technique to measure it.

v. Future experiments should involve more analysis of nanofibers mechanical testing. This could be accomplished by analyzing data from indentations occurring at different rates.

vi. Measure the Elastic Modulus of different diameter nanofiber and compare.

REFERENCES

1. Fibers, [Document posted on the Website of Department of polymer Science, University of Southern Mississippi] Retrieved on December 2003 from the World Wide Web. http://www.psrc.usm.edu/macrog/fiber.html. Accessed 10/03/2011

2. J. M. Deitzel, J. Kleinmeyer, D. Harris and N. C. Beck Tan (2001). The effect of processing variables on the morphology of electrospun nanofibers and textiles. Polymer, Volume 42(1), 261-272

3. Formhals A, Process and apparatus for preparing artificial threads. US Patent (1934), 1,975,504.

4. Baumgarten PK. (1971) Electrostatic Spinning of Acrylic Microfibers. Journal of Colloid and Interface Science, Vol. 36(1), 71-79

5. Larrondo I, Manley RS. (1981) Journal of Polymer Science: Polymer Physics Edition, 19, 909-20

6. Zheng-Ming Huang, Y.Z. Zhang, M. Kotaki, S. Ramakrishna(2003). A review on polymer nanofibers by electrospinning and their applications in nanocomposites; Composites Science and Technology 63, 2223-2253.

7. E.P.S. Tan, C.T. Lim. Mechanical characterization of nanofibers – A review Composites Science and Technology 66 (2006) 1102–1111.

8. Rayleigh, F. R. S., Phil., Mag. (1882) 44, p.184. Accessed 10/07/2011

9. Zeleny, J., Physical Review, (1914) 3, p. 69. Accessed 10/07/2011

10. Vonnegut, B., and Neubauer, R.I., Journal of Colloid Science (1952) 7, p. 616. Accessed 10/07/2011

11. Watchel, R.E., and Iamer, V.K., Journal of Colloid Science (1962) 17, p. 531. Accessed 10/08/2011

12. Taylor GI. Electrically Driven Jets. Proceedings of the Royal Society of London Series (1969) A Mathematical and Physical Sciences. Vol. 313, 453-475

13. Gladding, E.K., U.S Patent,(1939) 2,168,027. Accessed 10/15/2011

14. Simons H.I., U.S Patent,(1966) 3,280,229. Accessed 10/15/2011

15. Bomat A., U.S Patent, (1982) 4,323,525. Accessed 10/15/2011

16. Baumgarten PK (1971). Electrostatic Spinning of Acrylic Microfibers; Journal of Colloid and Interface Science, Vol. 36(1), 71-79

17. Larrondo, I., and Manley, R.ST.J. (1981) Journal of polymer physics Edition, Volume 63 p.909.

18. Kim J-S, Reneker DH. (1999) Mechanical Properties of Composites Using Ultrafine Electrospun Fibers. Polymer Science, 39(5) p. 849-854.

19. Doshi J, Reneker DH.(1995). Electrospinning Process and Applications of Electrospun Fibers; Journal of Electrostatics,35, 151-160

20. Srinivasan G, Reneker DH. (1995). Structure and Morphology of Small diameter Electrospun Aramid fibers; Polymer intemationa1, 36,195-201

21. Reneker DH, Chun I.(1996) Nanometer diameter fibers of polymer, produced by Electrospinning; Nanotechnology, 7, 216-223

22. Fang X, Reneker DH.(1997).DNA fibers by electrospinning; Journal of macromolecular science: Physics, Volume 36, Pages 1-428

23. Deitzel, J. M.; BeckTan, N. C.; Kleinmeyer, J. D.; Rehrmann, J.; Tevault, D. Army Research Laboratory Technical Report 1999, ARL-TR-1989

24. Yarin, A. L.; Koombhongse, S.; Reneker, D. H. J Applied Physics 2001, 89, 5.

25. Deitzel, J. M.; Kleinmeyer, J.; Harris, D.; BeckTan, N. C Polymer 2001, 42, 261

26. Ramkumar, S. S.; Sastri, L. ATA J 2002, Aug/Sep, 49.Warner, S. B.; Buer, A.; Grimler, M.; Ugbolue, S. C.; Rutledge, G. C.; Shin, M. Y. National Textile Center Annu Report November 1998, 83

27. Jaeger, R.; Bergshoef, M. M.; Batlle, C. M. I.; Holger, S.; Vancso, G. J. Macromol Symp 1998, 127, 141.

28. http://www.espintechnologies.com/ accessed 11/02/2011

29. http://www.donaldson.com/en/filtermedia/nanofibers/index.html accessed 11/02/2011

30. Gibson, P. W.; Gibson, H. L.; Rivin, D. AIChe J 1999, 45, 190.

31. Moses, M.; Hohman, M. M.; Shin, Y. M.; Rutledge, G. C.; Brenner, M. P. Phys Fluids 2001, 13, 2201.

32. Moses, M.; Hohman, M. M.; Shin, Y. M.; Rutledge, G. C.; Brenner, M. P. Phys Fluids 2001, 13, 2221.

33. Shin, Y. M.; Hohman, M. M.; Brenner, M. P.; Rutledge, G. C. Polymer 2001, 42, 9955.

34. Yarin, A. L.; Koombhongse, S.; Reneker, D. H. J Appl Phys 2001, 89, 301.

35. Shin, Y. M.; Hohman, M. M.; Brenner, M. P.; Rutledge, G. C. Applied Physics Letter 2001, 78, 1149.

36. Reneker, D. H.; Yarin, A. L.; Fong, H.; Koombhongse, S. J Applied Physics 2000, 87, 4531.

37. Fridrikh, S. V.; Yu, J. H.; Brenner, M. P.; Rutledge, G. C. Physical Review Letters, 2003, 90, 144502.

38. Megelski, S.; Stephens, J. S.; Chase, D. B.; Rabolt, J. F. Macromolecules 2002, 35, 8456.

39. Buchko, C. J.; Chen, L. C.; Yu, S.; Martin, D. C. Polymer 1999, 40, 739.

40. Deitzel, J. M.; Kleinmeyer, J. D.; Hirvonen, J. K.; BeckTan, N. C Polymer 2001, 42, 8163.

41. Atala, Mooeny et. al.(1997) Synthetic Biodegradable Polymer Scaffolds. Boston, MA: Birkhauser.

42. W.M. Saltzman, R.P Lanza, R. Langer, J. Vancanti, Editors , Principles of Tissue Engineering, (2nd edn.), Academic Press, California (2000), p. 221

43. Zheng-Ming Huang, Y.Z. Zhang, M. Kotaki, S. Ramakrishna (2003). A review on polymer nanofibers by electrospinning and their applications in nanocomposites; Composites Science and Technology 63, 2223-2253.

44. Matalov-Meytal, Y.; Sheintuch, M. Electrospinning of Nanofibers, Applied Catalysis A: General 2002, 231, 1.

45. http://www.donaldson.com/en/filtermedia dated 11/18/2011.

46. http://www.acell.com dated 11/18/2011.

47. Gibson, H.; Gibson, P. http://www.asc2004.com dated 11/18/2011.

48. Doshi, J.; Mainz, M. H.; Bhat, G. S. Nanofibers Nonwovens, Proceedings of the 10th TANDEC Conference 2000, Knoxville, TN.

49. Lee, Y.; Bhat, G. Processing and Fabrication of Advanced Materials for High Temperature Applications, Ed. T. S. Srivatsan and R. A. Varin; The Materials Society: Warrendale, PA, 2003

50. http://techreports.larc.nasa.gov/ltrs/PDF/2003/aiaa/NASA-aiaa-2003–1768.pdf accessed 10/16/2011

51. K.H. Ieea, H.Y. Kimb, M.S. Khilb, Y.M. Rab, D.R. Leeb(2003).Characterization of nano-structured PCL nonwoven mats via electrospinning; Polymer 44,1287-1294.

52. Perez-Rigueiro J, Viney C, Llorca J, Elices M. Silkworm silk as an engineering material. J Applied Polymer Science 1998; 70: 2439–47.

53. Yu MF, Dyer MJ, Skidmore GD, Rohrs HW, Lu XK, Ausman KD, et al. Three-dimensional manipulation of carbon nanotubes under a scanning electron microscope. Nanotechnology 1999; 10: 244–52.

54. Available from: http://www.zyvex.com Accessed 10/15/2011

55. Demczyk BG, Wang YM, Cumings J, Hetman M, Han W, Zettl A, et al. Direct mechanical measurement of the tensile strength and elastic modulus of multiwalled carbon nanotubes. Mater Science Eng A – Structure Mater Prop Microstructure Process 2002;334 (1–2): 173–8.

56. Tan EPS, Lim CT. A novel approach to tensile testing of micro- and nanoscale fibers. Rev Science Instrument 2004; 75(8):2581–5.

57. Namazu T, Isono Y, Tanaka T. Plastic deformation of nanometric single crystal silicon wire in AFM bending test at intermediate temperatures. J Microelectromech Syst 2002; 11(2):125–35.

58. Namazu T, Isono Y. Quasi-static bending test of nano-scale SiO2 wire at intermediate temperatures using AFM-based technique. Sensor Actuator A: Phys 2002; 104:78–85.

59. Ma PX, Zhang R. Synthetic nano-scale fibrous extracellular matrix. J Biomed Mater Res 1999;46:60–72

60. Cheng Zhu, G. B., and Ning Wang. (2000). "Cell Mechanics: Mechanical

Response, Cell Adhesion, and Molecular Deformation." Annual. Revised. Biomedical. Eng., 02, I89- 226.

61. Binnig, G. C. F. Q., and C. Gerber. (1986). "Atomic force microscope." Phys. Rev. Lett., 56, 930-933.

62. R. Wiesendanger, Scanning Probe Microscopy and Spectroscopy, (Cambridge: Cambridge University Press, 1994).

63. R. D. Piner, J. Zhu, F. Xu, S. Hong, and C.A. Mirkin, *Science* 283, 661 (1999) Accessed 10/24/2011

64. Y. Xia and G.M. Whitesides, American Chemical Society, *Langmuir* 13, 2059 (1997) Accessed 10/24/2011

65. Goodman, F. O. A. N. G. (1991). "Roles of the attractive and repulsive forces in atomic force microscopy." Physical Rev. B, 43, 4728-4731.

66. Lal, R., and Scott A. John. (I994). "Biological applications of atomic force microscopy." Am. J. Physiol., 266(Cell physiology. 35), C1-C21.

67. Butt, H. J. (1991). "Measuring electrostatic, van der Waals, and hydration forces in electrolyte solutions with an atomic force microscope." Biophys. J., 60, 1438-1444.

68. Hoh, J. H., J.P. Cleveland, C.B. Prater, J.P. Revel, and P.K. Hansma. (1992). "Quantized adhesion detected with the atomic force microscope." J. Am. Chem. Soc., 114, 4917-4918.

69. K Zeman, H. E. a. E. S. (1990). "Bending undulations and elasticity of the erythrocyte membrane organization." Europ. Biophys. J., 18, 203-219.

70. Dziedzic, A. A. a. J. (1989). "Internal cell manipulation using infrared laser traps." Proc. Natl. Acad. Sci., 86, 7914-7918.

71. K Svoboda, C. S., D Branton and SM Block. (1992). "Conformation and elasticity

of the isolated red blood cell membrane skeleton." Biophys. J., 63, 784-793.

72. H Luers, K. H., J Litniewski, J Bereiter-Hahn. (1991). "Acoustic microscopy of cultured cells. Distribution of forces and cytoskeletal elements." Cell Biophys, 18, 279 -293.

73. Rugar, J. H. a. D. (1984). "Measurement of cellular elastic properties by acoustic microscopy." J. Micros., 134, 245-260.

74. Radmacher, M. (1997). "Measuring the elastic properties of biological samples with the AFM." IEEE Eng. Med. Biol. Mag., 16, 47-57.

75. Pethica, J. B. 0, W.C. (1987). "Tip surface interactions in STM and AFM." Physica Scripta Volume T, Volume T19A, 61-66.

76. Colton, N. B. a. R. J. (1989). "Measuring the nanomechanical properties and surface forces of materials using an atomic force microscope." Journal of Vacuum Science & Technology A (Vacuum, Surfaces, and Films), 7(4), 2906-2913.

77. P. Maivald, H.-J. B., S.A.C. Gould, C,B. Prater, B. Drake, J.A. Gurley, V.B. Elings and P.K. Hansma. (1991). "Using force modulation to image surface elasticities with the atomic force microscope." Nanotechnology, 2(2), 103-106.

78. N.J. Tao, S. M. L. a. S. L. (1992). "Measuring the microelastic properties of biological material." Biophysical Journal, 63(4), 1165-1169.

79. A.L. Weisenhorn, P. K. H., T.R. Albrecht and C.F. Quate. (1989). "Forces in atomic force microscopy in air and water." Appl. Phys. Lett., 54(26), 2651-2653.

80. B. Cappella, P. B., C. Frediani, P. Miccoli and C. Ascoli. (1997). "Force-distance curves by AFM. A powerful technique for studying surface interactions." IEEE Eng. Med. Biol. Mag., 16(2), 58-65.

81. Costa, K. D. a. F. C. Y. (1999). "Analysis of indentation: implications for measuring mechanical properties with atomic force microscopy." J Biomech Eng, 121(5), 462-71.

82. Hertz, H. (1881). "Uber die beruhrung fester elastischer korper (On the contact of elastic solids)." J. Reine Angew. Mathematik, 92, 156-157.

83. Radmacher, M., Fritz, M., and Hansma, P.K. (1995). "Imaging soft samples with the atomic force microscope: Gelatin in water and propanol." Biophys. J., 69, 264- 270.

84. AL Weisenhorn, M. K., S Kasas, V Gotozos, MR Celio and HJ Butt. (1993), "Deformation and height anomaly of soft surfaces studied with the AFM." Nanotechnology, 4, I06-113

85. Butt HJ, Jaschke M. Calculation of thermal noise in atomic-force microscopy. Nanotechnology. 1995; 6:1–7.

86. Chen BY, Yeh MK, Tai NH. Accuracy of the spring constant of atomic force microscopy cantilevers by finite element method. Anal Chem. 2007; 79:1333–1338.

87. Clifford CA, Seah MP. The determination of atomic force microscope cantilever spring constants via dimensional methods for nanomechanical analysis. Nanotechnology. 2005; 16:1666 –1680.

88. Green CP, Cleveland JP, Proksch R, Mulvaney P, Sader JE. Normal and torsional spring constants of atomic force microscope cantilevers. Rev Sci Instrum. 2004; 75:1988 –1996.

89. Higgins MJ, Proksch R, Sader JE, et al. Noninvasive determination of optical lever sensitivity in atomic force microscopy. Rev Sci Instrum. 2006; 77.

90. Hutter JL, Bechhoefer J. Calibration of atomic-force microscope tips. Rev Sci Instrum. 1993; 64:3342–3342.

91. Neumeister JM, Ducker WA. Lateral, normal, and longitudinal spring constants of atomic-force microscopy cantilevers. Rev Sci Instrum. 1994; 65:2527–2531.

92. Sader JE. Parallel beam approximation for v-shaped atomic-force microscope

cantilevers. Rev Sci Instrum. 1995; 66:4583– 4587.
93. Sader JE, Chon JWM, Mulvaney P. Calibration of rectangular atomic force microscope cantilevers. Rev Sci Instrum. 1999; 70:3967–3969.

94. Senden TJ, Ducker WA. Experimental-determination of spring constants in atomic-force microscopy. Langmuir. 1994; 10:1003–1004.

95. Torii A, Sasaki M, Hane K, Okuma S. A method for determining the spring constant of cantilevers for atomic force microscopy. Measurement Science Technology. 1996; 7:179 –184.

96. Clifford CA, Seah MP. Quantification issues in the identification of nanoscale regions of homopolymers using modulus measurement via AFM nanoindentation. Appl Surf Sci. 2005; 252:1915–1933.

97. Muller DJ, Helenius J, Alsteens D, Dufrene YF. Force probing surfaces of living cells to molecular resolution. Nat Chem Biol. 2009; 5:383–390.

98. Noy A, Vezenov DV, Lieber CM. Chemical force microscopy. Annu Rev Mater Sci. 1997; 27:381– 421.

99. http://web.mit.edu/cortiz/www/nanomechanics.html Accessed 10/29/2011